UNIVERSITY OF ZIMBABWE

FACULTY OF ENGINEERING

DEPARTMENT OF CIVIL ENGINEERING

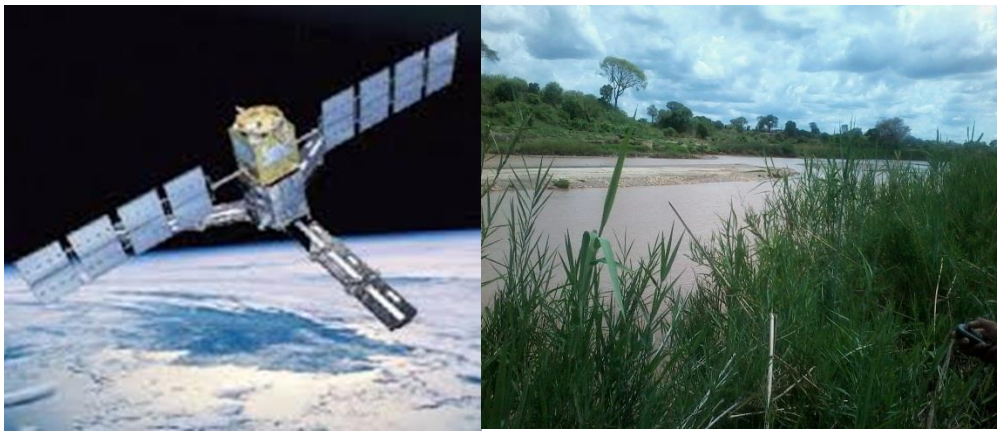

MODELING FLOODS IN THE MIDDLE ZAMBEZI BASIN USING REMOTE SENSING AND HYDROLOGICAL MODELING TECHNIQUES

By

TENDAI NHARO

Supervisors

Dr. Eng. H. MAKURIRA
Mr. W. GUMINDOGA

A thesis submitted in partial fulfillment of the requirements for the degree of Master of Science in Water Resources Engineering and Management of the University of Zimbabwe

JULY 2016

Declaration

I Tendai Nharo, declare that this study work is my personal work and it is submitted in the department of Civil Engineering for the Master degree in Water Resource Engineering and Management. This information has not been submitted before for any degree of examination in any other University.

Date

Signature:

Disclaimer

This research was carried as part of the curriculum of study at the University of Zimbabwe, Civil Engineering Department. Opinions, views and expressions in this work remain the sole responsibility of the author, and not necessarily represent those of the University.

Table of Contents

List of Figures

List of Tables

List of Equations

Dedication

To Shepherd Jisinawo and Chiwoneso Jisinawo

ACKNOWLEDGEMENT

I acknowledge Mr Shepherd Jisinawo for the financial provision throughout this study.

I extend my gratitude to Dr. Eng. H. Makurira and Mr. W. Gumindoga for their supervision and support in this research work. Special appreciations goes to the staff of the Department of Civil Engineering for conveying a great deal of knowledge to me. I am also thankful to the assistance from Mr Matawa.

I am greatly appreciative to my husband Shepherd Jisinawo, my daughter Chiwoneso and my parents Mr & Mrs Nharo for their moral and spiritual support. I have no words for my dear family members to mention, Tanaka Nharo. Thank you for being there for me all the time and the courage you have given me.

ABBREVIATIONS

AUC	Area under Curve
BLR	Binary Logistic Regression
CRED	Centre for Research on Epidemiology of Disasters
DBF	DataBase File
DD	Distance from dams
DEM	Digital Elevation Model
EVI	Enhanced Vegetation Index
GDP	Gross Domestic Product
Hec-HMS	Hydrologic Engineering Center- Hydrologic Modeling System
Hec-RAS	Hydrologic Engineering Center- River Analysis System
ILWIS	Integrated Land and Water Information System
*jpeg	Joint Photographic Experts Group
MODIS	Moderate Resolution Imaging Spectroradiometer
NDVI	Normalized Difference Vegetation Index
OFDA	Office of Foreign Disaster Assistance
OLI	Operational Land Imager
QGIS	Quantum Geographic Information System
RBMP	River Basin Master Plan
SADC	Southern African Development Committee
SCS	Soil Conservation Service
SDGs	Sustainable Development Goals
SRTM	Shuttle Radar Terrain Mission
SPSS	Statistical Package for the Social Sciences
TIFF	Tagged Image File Format
TPI	Topographic Position Index
UH	Unit Hydrograph
UTM	Universal Transverse Mercator
WMO	World Meteorological Organization
ZIMSTAT	Zimbabwe Statistics
ZINWA	Zimbabwe National Water Authority

Abstract

Mbire District, in the Middle Zambezi Basin, experiences floods annually. The study aimed at applying remote sensing and hydrodynamic modeling tools to map, and understand flood processes in order to improve flood management in the district. In determining the spatial and temporal variation of flood inundation in the district, NDVI MODIS images for the period 2005-2006, 2008-2009, 2013-2014 and 2014-2015 were processed in ILWIS GIS environment. The above period was classified by the Civil Protection Unit and ZINWA as flood years. Validation of the MODIS derived flood areas was done using 68 GCPs collected using participatory GIS mapping methods. A binary logistic regression model through the SPSS software was used to determine the spatial variation of flood hazard as a function of environmental factors. The results were confirmed using hydrologic modeling techniques, where the HEC-HMS model helped to quantify the peak flow and runoff contributed by the three sub-basins in the Mbire District (Angwa, Musengezi and Lower Manyame). The HEC-RAS model was used to map inundated areas for the Lower Manyame Basin for the flood return periods, 10, 25, 50 and 100 years. Flood mapping using MODIS images showed that the maximum areas flooded is 1 934 km^2 on 16 January 2006, and 1 895 km^2 on 8 January 2015. A good agreement of (R^2=0.86) between GCPs and MODIS derived flooded area for 8 January 2015 was recorded. Environmental factors that significantly explained flooding are distance from water bodies ($p<0.05$). Simulations through the HEC-HMS model indicated an average yearly observed flow rates of 15.6 * 10^7 m^3 16.2 * 10^7 m^3, and 25.7 * 10^7 m^3 for Lower Manyame (Mapomha), Musengezi (C109) and Angwa (Angwa) basins respectively. These flows were against an average discharge of 19.7 * 10^7 m^3 /yr., 18.3 * 10^7 m^3/yr. and 25.4 * 10^7 m^3/yr. for Lower Manyame, Musengezi, and Angwa respectively. Model performance was evaluated and the efficiency for Musengezi showed a RMSE of 5.25 %, RBIAS of 0.04 % for Angwa the RMSE was 3.94 % and RBIAS of -0.003 % and Manyame gave a RMSE of 5.25 % and RBIAS of 0.07 %. The HEC-RAS simulated inundated areas are 56.3 km^2, 57.3 km^2, 58.4 km^2, 58.7 km^2, 59.1 km^2 for the 2008-9 season, 10 year, 25 year, 50 year and 100 year return floods respectively and these are in and around Chikafa, Hunyani and Mushumbi Pools areas. The study concludes that Mbire District is vulnerable to floods hence the need for a flood protection measure framework that provides practical and feasible solutions, basic constructional guidelines for the protection of settlements and agricultural lands as well as a near real-time monitoring framework provided by this study.

Key Words: *Binary Logistic Regression, Flood routing, NDVI, Return Period, MODIS*

CHAPTER ONE: INTRODUCTION

1.1 Background

Flooding is a temporary covering of land by water normally not covered by water. Floods are among the most distressing and disastrous events affecting the human race. When a river over spills due to a lot of precipitation or inadequate channel size or obstructions within the river channel, floods occur (Nilsson and Berggren, 2000). Floods are also a result of back waters into branches and floodplains when the main river channel is in high stage (Madamombe, 2004).

Floods bring about, water-borne diseases such as dysentery, cholera and malaria. At the same time, communities benefit from floodplains when they practice floodplain agriculture were they do not have to apply fertilizers due to the nutritious sediments. For example the Mbire communities practice floodplain agriculture (Shumba et al., 2014). Floodplain farming is also common in the Limpopo Basin, in the Barotse floodplains in Zambia and floodplains in Mozambique (Emerton, 2003).

Yearly floods cause massive damage throughout the world (Ganova, 2003). The past 20 years has seen almost 100 000 people killed and in excess of 1.4 billion people affected by floods (Jonkman, 2005). The Asian continent is extremely vulnerable to flood events especially countries such as China, Philippines, India, Bangladesh and Nepal (Osti et al., 2008). On a global scale the most distinguished flood events have been recorded in Asia, South and North America and parts of Africa.

In Africa, flood events recorded between 1900 and 2006, showed that nearly 20 000 people were killed nearly, 40 million people affected and damages worth close to US$ 4 billion (Mulugeta et al., 2007). As stated by the United Nations (2009), torrential rains that occurred in 2009 resulted in floods that affected 600,000 people in 16 West African countries. Among the countries worst hit was Burkina Faso, Niger, Ghana and Senegal. The United Nations also highlighted the 2007 floods in the same African region that displaced more than one million

people in countries like Sudan, Ethiopia, Togo, Uganda, Bur- kina Faso, Mali and Niger. The floods killed in excess of 500 people.

According to a World Bank (2010) report, Southern Africa experienced floods in 2007 which affected more than 190 000 people. The floods affected countries such as Mozambique, Namibia and parts of Zambia. Southern Africa experiences flooding due to reservoir operations and cyclones and floods in the western parts of Africa are caused mainly by torrential rains (Beck and Bernauer, 2010).

Environmental degradation and climate variability have exacerbated the risk of annual flooding in the Zambezi Basin resulting in displacements of more than 100 000 people yearly (Madamombe, 2004). The Zambezi and Chobe Rivers' rise in water levels in 2010 led to severe floods in the Caprivi region, particularly Katima, Mlilo and Kabbe. An estimated 30 000 people in Oshana, 30 000 people in Kavango Regions and 50 000 people in Caprivi were affected as reported by The Disaster Relief Emergency Fund (2011). The Limpopo Basin experiences devastating floods for example the year 2000 floods killed about 500 people, and displaced more than 2 million people. A river part in Mozambique increased from 100 m wide to about 15 km wide for a stretch close to 100 km and inundated more than 1 400 km^2 of farmland (Shela, 2012).

The Mbire District (selected for this study) of the Middle Zambezi Basin in Zimbabwe experiences flooding despite the low rainfall and high temperatures for the area. With four major tributaries of the Zambezi River passing through the district, the district experiences flooding from the Cahora Bassa back-water flows. The Mbire district inhabitants experience seasonal floods and droughts in addition to the wild animals they have to coexist with (Beck and Bernauer, 2010).

Developments in Geographic Information System (GIS) tools and advances in Remote Sensing technology has improved the quick assessments of flood events, real time monitoring and early warning systems for flood events. GIS tools have been used to classify flood prone areas in communities. GIS tools use different geographical layers to develop flood prone areas by overlaying and intersecting the layers (Sanyal and Lu, 2004). Remote Sensing

techniques have been utilized in the development of comprehensive flood maps that are crucial for the development of hazard maps and for input to several types of hydrological models (Khanna et al., 2005).

Flood modeling describes the progression of flooding incorporating the analysis of parameters and data representing flood settings (Costabile and Macchione, 2015). According to the World Meteorological Organization (2013) the analysis of flood model data and parameters may cover a river basin, a flood plain, an alluvial or is along an individual river section. The development of a River Basin Management Plan (RBMP) calls for the need to support environmental development selections incorporating prediction and simulation models. Hydrological simulation models are tools used to estimate the basin's hydrological reaction due to precipitation (Halwatura and Najim, 2013).

Flood risk management has many components and among them are the hydrological models. The hydrological models use precipitation and runoff which is routed to the outlet of the drainage basin (Zazo et al., 2015). The output of the model is a hydrograph which displays the peak flows and time to peak can thus be determined (Bengtson and Padmanabhan, 2000). A hydraulic model uses the result from the hydrologic model and comprehensive information about the geometry of flow cross sections to define flood-plain boundaries (Papathanasiou et al., 2015). Therefore communities should invest in these flood mapping and modeling technologies to help quantify the magnitude and extent of floods so that they are better prepared for flood disasters.

1.2 Problem Statement

Floods pose a serious threat to the sustainable management and development of the Zambezi River Basin because of their destructive nature. The Cyclone Eline floods of 2000 in the Zambezi Basin left 700 people dead and over 500 000 homeless as cited by Tumbare (2004). The Mbire District in the Zambezi Basin is flood prone and the communities are affected by floods almost every year. The problem in mitigating floods is associated with the fact that it is not known to what extent environmental factors contribute to floods. Previous studies in the District by Muhonda et al. (2014), Shumba et al. (2014) and Bola et al. (2014) focused on

causes, costs and benefits of these floods including coping mechanisms. To the best of our knowledge, no study in the District has mapped flood inundation areas in addition to explaining the relationship between levels of inundation and environmental factors. This research seeks to combine and apply Remote Sensing, geostatistical techniques and hydrological modeling techniques to better understand flood processes in the district and to improve the efficiency of flood management in the Zambezi Basin at large.

1.3 Justification

Sustainable Development Goals (SDGs) support the need for disaster risk reduction, early warning systems, adaptation to climate change and strengthened resilience. There is need to support the goals in Mbire District by mapping flood inundation over time by applying near real-time satellite data. District authorities need to measure the development of floods and quantify the severity of the state and damage caused by floods. Therefore, there is need to use GIS and Remote Sensing tools for hydrologic modeling and measuring flood inundation to effectively analyse flood events as well as mapping flood areas in the Mbire District.

1.4 Objectives

1.4.1 Main objective

To model floods in the Middle Zambezi Basin using remote sensing and hydrological modeling techniques.

1.4.2 Specific Objectives

i. To determine the spatial and temporal variation of flood inundation areas in the Mbire District using remote sensing
ii. To explain the factors affecting flood magnitude and extent in the Mbire District using existing geostatistical models
iii. To use hydrological modeling tools for flood mapping in the basin.

CHAPTER TWO: LITERATURE REVIEW

2.1 Introduction

This section reviews literature on flood modeling. The section starts with definitions and causes of floods, analysis of occurrence of floods and finally hydrological models as found in literature.

2.2 Analysis of floods

A flood is the inundation of a region, usually dry caused by a rise in water levels of a river channel and the channel running out of its confinements (Leonard, 2009). Some writers say a substantial amount of rainfall cause flooding however, floods can result from ways that are not directly linked to ongoing meteorological events. According to Nelson (2001) floods are caused by meteorological events, hydrological and anthropogenic activities. Meteorological causes are a result of prolonged and extreme rainfall, storms, monsoons and cyclones (Ganova, 2003).

Hydrological causes of flooding include increased runoff from snow and ice melt down, impervious surfaces, waterlogged soils, poor permeation rates and land erosion. Anthropogenic causes, are associated with land use changes which include, deforestation, intensive agriculture and unplanned flood control events (Cupal et al., 2015).

Constant flood cycles of floodplain ecosystems are essential in maintaining the ecological integrity and biodiversity of these areas (Garcia et al., 2015). Anthropogenic activities in these systems has altered the extent, occurrence, and period of floods, and as a result the interactions of water, nutrients, sediments, and biota between the floodplains and river has been modified (Thoms et al., 2005). Floodplains help in river flood attenuation understanding their inundation dynamics is critical for decision making on flood risk management (Bates et al., 2006).

2.2.1 Flood dynamics on a global scale

Globally, the frequency and rate of flood occurrences is on the rise (Muhonda et al., 2014). Statistics taken between the year 1991 and 2005, revealed that approximately 3 300 floods were reported worldwide, accounting to 64 % of all natural tragedies in that period (Rodriguez et al., 2009). Geographic location and climatic conditions makes some regions in the world more vulnerable to floods. According to the World Bank (2006) the Asian continent is the most vulnerable to flood occurrences.

In the year 2010, heavy floods occurred in Pakistan, India and China. In Colombia, the floods occurred between October and December 2010 and in Australia floods occurred during the austral summer of 2010/11. As cited by Kundzewicz et al. (2014), the estimated damage caused by these floods in China alone, where a total loss of US $51 billion. In Pakistan, close to 2000 fatalities from the monsoonal flooding were recorded. Year 2011, Africa experienced severe floods in Namibia, Mozambique, South Africa and Uganda. In America, 2011 had floods in countries like Brazil, Columbia, Mexico and the United States in the Americas. In the Asian continent, Cambodia, China, India, Korea, Pakistan, the Philippines and Thailand had floods in 2011. The 2011 floods had fatalities in each event of over 50 and damage to property particularly in the developed countries (Jonkman, 2005).

The year 2012 had severe floods again with more than 50 fatalities recorded from the countries, Niger, Madagascar, and Nigeria in Africa; China, Bangladesh, India, North and South Korea, the Philippines and Russia in Asia; and Argentina, the United States and Haiti in the Americas (Kundzewicz et al., 2014).

2.2.2 Floods in Southern Africa

In Southern Africa floods are common events that damage agricultural fields, infrastructure, displace people and threaten lives. Studies done in Southern Africa on floods predict a rise in frequency and intensity of these hydro-meteorological events due to climate variability (Jovel et al., 2009). The preceding two decades (1994 to 2014) has recorded some of the worst floods in Southern Africa for example the year 2000 flood in Mozambique (Muhonda et al.,

2014). According to a World Bank (2006) report, the Mozambique flood had an estimated cost of $550 million and lowered the countries' GDP growth rate from 7.5 % to 1.5 %. The negative impacts of floods in Southern Africa lead to food insecurity, loss of livestock and human lives (Madamombe, 2006).

March 2009 had torrential rains across Angola, Namibia and Zambia. The rains resulted in a rise in water levels in the Kunene, Chobe, Zambezi and Okavango Rivers to a point that the north-eastern and north-central regions of Namibia experienced the worst flooding in years. The flood induced destructions affected almost 60 % of the population in that area. Communities were displaced, crops and livestock washed away and infrastructure damaged (Jovel et al., 2009).

The Shire Basin has also experienced devastating floods. A study by Mwale et al. (2015) in the Lower Shire Valley in Malawi concluded that the region is predominantly in the medium to high vulnerability classes with respect to flood hazards. In the Limpopo River floodplain area, 11 flood events were recorded during the last century: AD 1915, 1937, 1955, 1967, 1972, 1975, 1977, 1981, 2000, 2012 and 2013 (Sitoe et al., 2015). The floods were recorded in newspapers, recorded in reports from Direcção Nacional de Águas as well as from observations. The Limpopo Basin floods are caused by flash floods when upstream dams are released in times of high flows as a way of protecting the hydraulic structures.

2.2.3 Floods in the Middle Zambezi River Basin

In 2007, cyclone induced floods occurred in the Zambezi Basin, and displaced close to 56 000 households in Mozambique (Artur and Hilhorst, 2014). Muzarabani District in the northern Lowveld of Zimbabwe and within the Zambezi Basin experiences recurrent floods. The flooding is more severe in the Chadereka and Dambakurima areas of the district. The worst floods were experienced between 2001 and 2010 with the years 2000 and 2003 floods induced by cyclones (Mavhura et al., 2013). Floods experienced in the Muzarabani District are seasonal floods occurring between December and February, cyclone –induced floods and

floods due to dam releases from Kariba dam, upstream of the district or Cahora Bassa which is downstream.

Mbire District in Zimbabwe is also in the middle of the Zambezi Basin and receives an average annual rainfall of about 655 mm (Muhonda et al., 2014). Rainfall is irregular and floods are recurrent. The past two decades has seen the basin experiencing the worst floods. A lot of research in the area has been done to infer the causes of these floods, coping mechanisms as well as the impacts caused by these floods. Two types of floods affect the Mbire District, flash and cyclone induced floods between January and February (Madamombe, 2004) and the backwaters from the Cahora Bassa hydropower dam (Phiri, 2011).

Most of the seasonal floods experienced in the Mbire District are believed to be caused by flows from upstream catchment area. Occurrence of floods in the basin negatively impact on food security and livelihoods (Muhonda et al., 2014). Contrary to that, Shumba et al. (2014) found out that the communities have seen the hydrological benefits that can be derived from these floods. These floods bring about alluvium deposition which is very good for crops as well as the wetness in the floodplains is an advantage to farmers who practice recession farming Recession agriculture is a farming practise which uses remaining moisture of seasonally flooded areas when the floods recede (Beilfuss, 2001).

2.3 Factors affecting flood occurrence and magnitude

2.3.1. Channel geometry and geology

When a stream runs out of its confines and submerges close areas a flood is experienced (Nelson, 2012). From a geographical perspective, floods are a natural outcome of river flow in a frequently changing environment. Extreme floods alter a river in-channel scour as well as changing the distribution of sediments. This change in the geometry of the river channel geometry lead to substantial effects on flood hydraulics and hence flood hazard (Guan et al., 2016).

The in-channel erosion due to extreme floods sometimes separates the waterway from its floodplains resulting in a decrease of floodwater storage and flooding will then occur. Geology can play a vital role in a flood with plastic soils such as sodic soils reducing infiltration and resulting in an increase in overland flow (Adejeji and Salami, 2008). Soil moisture affects the rate of infiltration and moisture content is inversely proportional to the rate of infiltration.

Distance from river networks and distance from reservoirs

High tides induce flooding in areas close to coastlines and along rivers. The study by Phiri (2011) in the Middle Zambezi Basin, areas covering Mbire District and parts of Mozambique found that reservoir operations of releasing water negatively affected communities living close to the reservoirs. The operations of the reservoirs are standard operations in times of high flows to save the hydraulic structures. Thus dams overflow with the sudden release of water into the downstream drainage and at times causing flooding (Mavhura et al., 2013).

Elevation and land cover changes

Low lying areas are at a threat of flooding than areas at a higher elevation (Adejeji and Salami, 2008). Land cover alterations changes the hydrological processes over a range of spatial and temporal scales. The landcover changes are linked to the amount of runoff generated as well as altering the hydrological factors that include interception, infiltration and evaporation (Ganova, 2003). Thus landcover changes lead to the changes in the occurrence and intensity of flooding. As concluded by Chen et al. (2009) in their study on impacts of landuse changes in Xitiaoxi, China, the future land cover change scenarios are projected to increase the total runoff as well as peak discharge.

2.4 Methods to map and model floods

Models and systems allowing flood risk output predictions incorporating GIS, Remote Sensing, hydraulic modeling and hydrologic models are in existence (Merkuryeva et al., 2015). GIS is used in processing as well as manipulating different types of spatial data for the

strategic flood hazard evaluations and relating to hydrodynamic flood modeling skills. A lot of studies have been done globally in modeling floods. Of note is work by Costabile and Macchione (2015), who mapped and modeled floods along the Crati River in Italy the river runs through a small town. GIS has many applications including storing and handling hydrological data and generating flood inundation and hazard in flood risk mapping (Evans et al., 2007).

2.4.1. Remote Sensing in flood area delineation

Landsat Missions

Landsat Multi Spectral Scanner (MSS) was the initial data available of satellite remote sensing with a resolution of 80 m. In the 1970s, the MSS data was applied in flood affected regions of Iowa, Arizona and Mississippi River Basin (Sanyal and Lu, 2004). Band 7 (0.8 – 1.1 μm) of the MSS was predominantly used for differentiating water and moist soil from non-water surfaces. The MSS band 7 has a strong absorption of water in the near infrared range of the spectrum (Smith, 1997).

The early 1980s saw the Landsat Thematic Mapper (TM) imageries with 30 m resolution used to monitor floods as well as separating inundated areas. The Thematic Mapper used band 4 to separate water from dry land because of its close equivalence to the MSS band 7 (Wang et al., 2002). Landsat MSS was used by Simpson et al. (2008) where they distinguished snow from clouds by estimating the areal extent of snow cover.

Wang et al. (2002) mapped the flood extent in the coastal floodplains of Pitt County using Landsat TM and DEM data in North Carolina USA. The method used in the study, used reflectance features of non-water against water targets on Landsat 7 Thematic Mapper (TM) images. Their results showed that 237.9 km^2 or 14 % of the total county was flooded. The study concluded that Landsat 7 images are reliable and could be used in other coastal floodplain regions.

Table 2.1 shows a summary of the temporal, spectral and spatial resolutions of the Landsat Missions

Table 2.1: A summary of the Landsat Missions

	Multi Spectral Scanner (MSS) Landsat 1-5	**Thematic Mapper (TM) Landsat 4 and 5**	**EnhancedThematic Mapper Plus (ETM) Landsat 7**
Spectral Resolution (μm)	0.5 -0.6 (green) 0.6 – 0.7 (red) 0.7 – 0.8 (NIR) 0.8 -1.1 (NIR)	1. 0.45 -0.52 (BLUE) 2.0.52-0.60 (GREEN) 3.0.63 -0.69 (RED) 4. 0.76 -0.90(NIR) 5.1.55 -1.75(MIR) 6. 2.08-2.35(MIR) 7. 10.4-12.5 (TIR)	1. 0.45 -0.52 2.0.53-0.61 3.0.63 -0.69 4. 0.78 -0.90 5.1.55 -1.75 6. 2.09-2.35 7. 10.4-12.5 8. 0.52-0.90 (Pan)
Spatial Resolution (m)	80*80	30*30 120*120 (TIR)	15*15 (Pan) 30*30 60*60 (Pan)
Temporal Resolution (revisit in days)	18	16	16
Spatial coverage (km)	185*185	183*170	185*185
Altitude (km)	915 (Landsat 1, 2, 3)	705	705

SPOT

SPOT (Satellite Pour l'Observation de la Terre) multi spectral images were used after the Landsat Missions. The images are commercial high resolution optical images. SPOT satellites offers revisit times and acquisition such that imagery is acquired every day anywhere in the world. Some of the SPOT imagery applications include flood delineation assuming that water has very low reflectance in the near infrared of the spectra. SPOT images together with a DEM were used in Bangladesh (Islam and Sado, 2000) to delineate monsoon floods. In Saudi Arabia, SPOT images and SRTM DEMs were used to generate flash flood maps for the city of Najran where the factors considered in the study to cause floods were, landuse, drainage density, soil type, runoff, surface slope, surface runoff and distance from the main channel (Elkhrachy, 2015).

Advanced Very High Resolution Radiometer

Advanced Very High Resolution Radiometer (AVHRR) images are coarse in resolution and usually contaminated by cloud cover. AVHRR temporal resolution is very high such that the images have been used in monitoring the progression of a flood in near real-time (Lawal et al., 2011). The Normalized Difference Vegetation Index (NDVI) is used together with AVHRR to monitor floods. When a surface is flooded, its NDVI value deviates from its known state. These images were applied by Wang et al. (2002) where he was observing the lower reaches of the Yangtze River USA, and concluded that the NDVI value for the inundated surface areas is negative while that for dry areas is greater than zero.

Synthetic Aperture Radar

A lot of cloud cover impedes the capture of flood progress in bad weather. Microwave remote sensing was developed especially the radar imageries to solve the cloud cover problem as they can penetrate cloud cover. Synthetic Aperture radar (SAR) is used in flood management due to its accuracy in differentiating land and water. The SAR images combined with optical images have been used to map urban impervious surfaces in China (Zhang et al., 2014). In Mozambique, Vilches (2013) used SAR images to detect areas affected by flooding they concluded that SAR images must be combined with optical imaging in estimating the depth of flooded areas.

Moderate Resolution Imaging Spectroradiometer

The Moderate Resolution Imaging Spectroradiometer (MODIS) is a spectrometer with total of 36 bands. MODIS is used in flood area delineation. MODIS provides a global data set every 1-2 days with a 16-day repeat cycle. The spatial resolution of MODIS (pixel size at nadir) is 250 m by 250 m for channel 1 and 2 (0.6 µm - 0.9 µm), 500m by 500m for channel 3 (0.45 µm -0.48 µm) (*(http://modis.gsfc.nasa.gov/)*. 2008).

MODIS has vegetation indices made up of two vegetation index products, the Normalized Difference Vegetation Index (NDVI) and Enhanced Vegetation Index (EVI) (Reed et al., 2009). The MODIS has many products including the highest resolution available in this

spectrometer, the 250 m spatial resolution 16-day compositing interval product. The compositing process uses a controlled view-angle, maximum value method, which retains the maximum vegetation index value over the 16- day period, provided that it meets a filtering condition based on cloud cover, quality, and viewing geometry (Reed et al., 2009).

MODIS was used in a study by Dottori et al. (2016) were they developed a global flood hazard mapping framework. MODIS was coupled with Global Flood Awareness System (GloFAS) in simulating the hydrological responses in the study area.

2.4.2. Hydrologic flood modeling

Hydrologic models are conceptual illustrations of a portion of the hydrological cycle. These models are used to forecast and understand the hydrological progressions. The models are separated in two, where the first type is called the stochastic hydrologic model (Nath et al., 2013). The stochastic model are built on statistical and mathematical concepts and are black box system. The second type of model is the deterministic hydrological model. These models are process-based representing the physical process as observed in real time. The drawbacks in these models is that they require a lot of data, storage space as well as time consuming (Xu, 2002). A lot of watershed models exist with many of the models applied to an array of problems. Hydrological models are distributed in space and time and are used to tackle environmental problems (Karmakar, 2010).

Stochastic models

Stochastic (statistical) models take into consideration the uncertainties in the input data as well as parameters. Statistical analysis methods include binary logistic regression, linear regression, double mass curve analysis and flood frequency analysis. Miller and Frink (1984) applied statistical analysis techniques to study how landuse changes affected the flood response in the Red River Valley Basin in North Dakota, Minnesota. Regression analysis of streamflow with time, precipitation and drainage area was also used by Daniel and Vining (1983). The study determined if streamflow had increased with time with increase in drainage area due to increased agricultural land drainage and precipitation.

Continuous probability distributions have been applied in the analysis of flood frequencies. A number of statistical distributions exist like the normal distribution which has two parameters, the mean (μ) and the standard deviation (σ). Some of the distributions are used in hydrological applications like the Pearson Distribution, the Lognormal Distribution, the Gamma distribution and Extreme value distributions. Extreme value distributions (Type I, II, III) are centred on the principle of extreme values which implies that if a random variable *T* is a maximum in a sample of size *n* from some population of *x* values then on condition that *n* is sufficiently large the distribution of *T* is one of the asymptotic types, depending on the distribution of *x*. The Type 1 distribution is the Gumbel distribution which was used by Mujere (2011a) to predict frequency of floods in Nyanyadzi River, Zimbabwe.

Deterministic models

Deterministic models describe the performance of hydrologic processes in a watershed by means of mathematical equations. Calibration of the models is done by comparing simulated results with existing data (Bengtson and Padmanabhan, 2000). Examples of deterministic models include HEC-1 Flood Hydrograph Package (HEC-1), HEC-HMS a later version of HEC-1, Hydrological Simulation Program – FORTRAN (HSPF), Precipitation – Runoff Modeling System (PRMS), EPA Storm Water Management Model (SWMM), DRAINMOD, and Agricultural Nonpoint Source Model (AGNPS). Ogawa and Male (1986) used HEC-1 and HEC-2 models in evaluating the potential of wetlands to mitigate flooding.

HEC-1 and AGNPS are categorised as event- simulation models and are applied in modeling single rainfall- runoff events using hourly or minute time intervals and generating peak flows. HSPF, SWMM, and PRMS are continuous models run in two time scales in the simulation, daily and storm mode having a shorter time step, an hour or less (Bengtson and Padmanabhan, 2000). Nath et al. (2013) used HSPF in simulations of the dynamics of phosphorus in floodplain wetlands in South Florida as well as assessing wetland restoration. Phiri (2011) used HEC-HMS in the Mbire District where he simulated flows from ungauged catchments.

HBV model

Hydrologiska Byråns Vattenbalansavdelning (HBV) is a model used in the analysis of river discharge and water pollution. HBV is found in many versions including HBV light. In modeling discharges, the model consists of routines for example, the soil moisture routine, snow routine, routing routine and response routine (Abebe et al., 2010). Inputs to the model include daily temperature, rainfall and evaporation. The model incorporates reservoirs, surface runoff and groundwater flow. Table 2.2 gives a summary of the hydrologic models

Table 2.2: Examples of hydrologic models

Model type	**Example**
Lumped parameter	Snyder Unit Hydrograph
Distributed	The Kinematic Wave
Event	HEC-HMS, SWMM, SCS TR-20, HEC-1
Continuous	SWMM, HSPF, STORM,
Physically based	HEC-HMS, HEC-1, SWMM, HSPF
Stochastic	Regression
Analytical	Rational method
Numerical	Dynamic wave models

Table 2.3 gives a summary of the hydrologic models and areas they are applied.

Table 2.3: Applications of the hydrologic models

Model	**Area applied**
Hydrologiska Byråns Vattenbalansavdelning (HBV)	Used in flow forecasting
HEC-HMS	Quantifies flows for drainage system designs
	Quantify the effect of land use change on flood
TOPMODEL and MIKE SHE (Système Hydrologique Européen)	Hydrologic simulation
National Weather Service (NWS)	Used in flood forecasts
Run-off routing model (RORB)	Flood forecasting, evaluation of the effect of land use change
Modular Modeling System (MMS)	Water resources management and planning activities

Hydraulic modeling

Numerous model constructions have been established to calculate flood inundation. One-dimensional (1D) flow routing methods such as LISFLOOD, Mike 11, ISIS or HEC. St.

Venant/Shallow Water Equations are traditional numerical hydraulic models used in practical river engineering (Pappenberger et al., 2005). 1D models are (in comparison to higher dimensional models) easier in application and do not require a lot of data and computer power (Pappenberger et al., 2005).

Hydraulic models are used to compute and analyse water surface profiles, 3D views of channels, stage along a river. The models are used to define areas inundated by flood flows. There are specialised hydraulic models used in predicting effects of numerous obstacles in the over bank areas like weirs, bridges and culverts. HEC (US Army Corps of engineers-Hydraulic Engineering Center) is a typical specialised hydraulic model which has numerous types and several couplings to analysis tools ((HEC), 2008). HEC-RAS was used by Azagra and Olivera (1999) in calculating inundated area for Waller Creek in USA. Heimhuber (2013) estimated the flood risk of Onaville in Haiti using HEC-HMS and HEC-RAS.

The 2D depth-averaged and 3D models are suitable for hydrological applications but their computational demands limit their application over the very large space and time scales typical of huge river-floodplain systems. 2D models have been successfully applied in real-world applications Nevertheless these models require very high computational costs when applied in high resolution grid (Garcia et al., 2015). There are many conditions in which the computational resources of 2D models becomes prohibitive resulting in the adoption of computational efficient flood inundation models. Lately there has been substantial interest in simulating river hydraulics at regional to global scales, for the purpose of flood risk and flood hazard assessments (Neal et al., 2015).

CHAPTER THREE: MATERIALS AND METHODS

3.1 Description of study area

Mbire District is one of Zimbabwe's 64 districts located between 30.60° and 31.20° east and 15.60° and 16.40° south. The district has an estimated land area coverage of 4700km^2 at an average elevation of 550 meters above mean sea level (Bola et al., 2014). The main rivers within the district are Musengezi, Manyame, Kadzi, Angwa and Mwanzamutanda which all drain into Zambezi River (Figure 3-1).

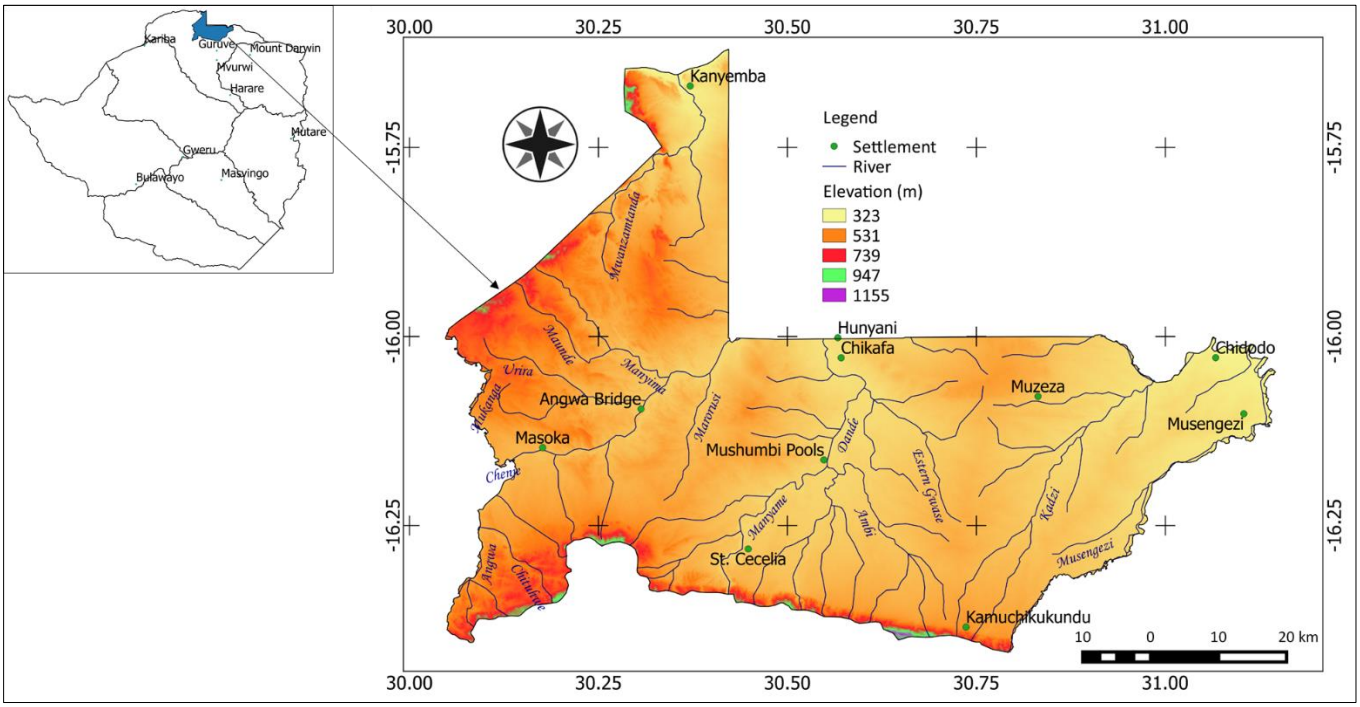

Figure 3-1: Mbire District showing the main centres and rivers

3.1.1 Climate

Mbire District lies in region IV which is one of the five natural agro-ecological regions in Zimbabwe. The region is characterised by low rainfall, approximately 650 mm per year (Muhonda et al., 2014). The rain season starts in October to March but due to climate variability the seasons have changed with rains starting as late as November to early December or late January up to late March (Shumba et al., 2014). The months of September,

October and November are the hottest with maximum temperatures exceeding 40 °C (Kampata et al., 2008).

3.1.2 Soils and Geology

Mbire District lies on sedimentary geological foundations of lime and sandstone formations. Varied soils rich in sodium exist though lacking in organic matter (Shumba et al., 2014). The soil types are acidic, of high erosive potential and leached out (Dube et al., 2014). According to the Food and Agricultural Organization (2015) the common soil type in the study area are the Chromic Luvisols, Lithosols and Ferric Luvisols found in Angwa, Lower Manyame and Upper Musengezi.

3.1.3 Drainage

Mbire District is in a valley (average elevation of 550 m with a high of 763 m and a low of 337 m) with four main rivers from upstream flowing through and discharging into Zambezi River and Cahora Bassa. The district frequently experiences localised floods as a result of backflows from Cahora Bassa when it reaches a threshold of 328 m as concluded by Phiri (2011). These floods come about especially when the dam levels concur with large inflows from upstream contributions in the Manyame Catchment. The district is also bordered upstream by Kariba Dam and downstream by Cahora Bassa Dam.

3.1.4 Socio –economic profile

According to Zimbabwe Statistics (ZimStat) (2012) Mbire District has 17 wards, approximately 21 500 households and a population close to 116 000. Cotton growing is the chief economic activity in the area. People practise recession farming in the floodplains which gives them the possibility of a second harvest in one season.

From October to March, communities move off the floodplains and settle on higher ground and grow crops. Soon after the rains, they move back to the floodplains and grow maize, sweet potatoes, legumes which they harvest from September to October. Structures built in

the floodplains are make shift homes from dried grass. Livestock is another source of wealth among the Mbire communities.

3.2 Methodology for flood inundated area analysis

3.2.1 Data acquisition

This study used readily available MODIS NDVI flood images (NASA.GOV, 2010). The spatial resolution of band 1 and band 2 is 250m at nadir and a radiance between 620-670nm (visible red) and 841-876nm (near infrared) respectively, hence the suitability of these bands in flood water mapping. In addition, their moderate spatial resolution of 250 m was considered appropriate in this study for mapping the large area of the district of size 4700 km^2.Terra and Aqua's orbiting about the Earth is programed such they pass from north to south across the equator in the morning for Terra, while Aqua passes south to north over the equator in the afternoon (Dottori et al., 2016). Terra MODIS and Aqua MODIS view the entire Earth's surface every 1 to 2 days hence all flood events can be tracked.

A total of 39 MODIS NDVI flood images were downloaded from the MODIS Rapid Response System via the Internet www.nasa.gov. These were acquired between December and March for each season according to evidence of seasons that experienced floods acquired from the Zimbabwe National Water Authority (ZINWA) and Civil Protection Unit (CPU). The seasons are 2005-2006, 2008-2009, 2013-2014 and 2014-2015.

3.2.2 Validation of MODIS derived flooded areas

The validation of the MODIS derived flooded areas was done by GIS participatory mapping (Kindon et al., 2010). The technique is used to obtain evidence and henceforth produce maps which represent local knowledge and information. Participatory mapping is a method that was used in this study to obtain ground truthing data. Data was collected with the help of key people describing the areas flooded between the 24th and the 25th of December 2015 in

Chidodo, Mushumbi Pools, Chikafa and Masoka. A total of 68 ground control points (GCPs) were collected in the study area using the Global Positioning System (GPS). The GCPs were converted into a point map which showed the two classes of flooding and non-flooding.

Using the 'Map Value' function, the image showing presence of flooding for 2014-2015 season was used. Results in an ILWIS table format were exported to the Statistical Package for the Social Sciences (SPSS). In SPSS analysis tests were carried out to measure the agreement of the ground control points and the MODIS derived flooded area. Measure of agreement was first carried out using Area under the Curve (AUC). To confirm the robustness of the test, the Cohen Kappa Test was performed (Lydersen, 2014).

3.3 Methodology for assessing factors affecting flood magnitude

In this study, environmental factors affecting occurrence, presence and hence magnitude of floods were processed.

Satellite Images

Images from the MODIS derived flooded area showing presence and absence of water were used. A slope map, vertical channel distance, elevation map, and distance from rivers maps were derived from the DEM Hydroprocessing. The landcover maps were developed from, cloud free Landsat 8 OLI and TM images acquired from the GloVis website (www.earthexplorer.usgs.gov) for the hydrological seasons, 2005-2006, 2008-2009, 2013-2014, 2014-2015.

The images downloaded for each season were for April and September of each year prior to floods using Path/Row 170/71. Table 3.1 shows the details of the specification of data used in the land use classification.

Table 3.1: Landsat images used in classification

Year	Landsat sensor	April date of acquisition	September date of acquisition
2005	Landsat 5 TM	12 April 2005	19 September 2005
2007	Landsat 5 TM	2 April 2007	25 September 2007
2008	Landsat 5 TM	21 April 2008	12 September 2008
2013	Landsat 8(OLI)		25 September 2013
2014	Landsat 8(OLI)	21 April 2014	28 September 2014

3.3.1 Quantification of environmental factors

DEM Hydroprocessing

The digital elevation model (DEM) for the study area was used to derive the slope, river network and elevation for the model. The DEM image was obtained using the Shuttle Radar Terrain Mission (SRTM) output available with 30 m spatial resolution. The DEM was used to calculate flow direction, flow accumulation, network and catchment extraction. The first step in the preparation of the DEM was sink filling. Sinks result in an irregular flow grid direction which causes problems in processing (Maathuis, 2006).

Flow direction is the route water takes as it flows from pixel to pixel from the steepest slope. The flow direction computations were carried out to determine the flow accumulation. Flow accumulation calculated all the upstream water available for runoff. The flow accumulation data was used in defining watershed boundaries and stream networks (Gumindoga, 2008). Using the stream network map, a distance computation was done assigning to each pixel the least distance to the closest stream. Slope was calculated (Equation 1) as a percentage with pixel size of 30.

Equation 1

*Slope = 100 * HYP (DDFDX, DDFDY)/30*

where: DDFDX = change in the horizontal direction

DDFDY = change in the vertical direction

Distance from water bodies

Using QGIS and Bing Aerial imagery, dams in and around the district were digitized as a polygon shapefile and georeferenced to UTM zone 36S. The shapefile polygon was exported to ILWIS and converted to raster thus facilitating a distance calculation operation to be carried out. The map was resampled to the extent of Mbire District. Distance from rivers was also calculated using the segment map of rivers obtained through DEM Hydroprocessing. The distance from rivers map was rasterized and resampled to the study area.

Topographic Position Index

The Topographic Position Index is an algorithm used to calculate topographic slope positions and to automate landform classifications. Using QGIS, the raster tool, analysis and DEM terrain model was selected to compute TPI (Equation 2) using the same SRTM dem (Aryal and Bates, 2008).

Equation 2

Tpi <scalefactor> = int ((dem – focalmean (dem, annulus, irad, orad)) +5

where scalefactor = outer radius in map units

Irad = inner radius of annular in cells

Orad = outer radius of annular in cells

Soils

The soil map obtained from the Harmonized World Soil Database classification was extracted for the district ((FAO), 2009).

Vertical channel distance

The DEM and rivers obtained from DEM Hydroprocessing were converted to a point map in a GIS environment. The nearest point calculation was carried out to obtain the channel base elevations which were used to form a channel height layer that. The channel height layer was subtracted from the DEM to produces the vertical distance to the closest channel of each

location in the study area. The vertical height above the nearest channel was then determined by subtracting the channel base height interpolation from the original DEM:

DEM – Channel height = vertical channel distance

Landcover

The Integrated Land and Water Information System (ILWIS 3.31 academic) was used to carry out the spatial analysis of the raw Landsat images. The images were imported into ILWIS in GeoTiff format via the Geo-gateway, an in-built ILWIS function that ensures compatibility. For Landsat TM, *band 2, band 3* and *band 4* were imported and converted to ILWIS formats. Proper Georeference was assigned for each band and stretched using the linear 2 % option. A maplist was created using bands 2, 3 and 4 for visualisation in false colour.

The bands were opened as false colour composites so as to improve visual interpretation of features. A sampleset was created based on image interpretation, based on the spectral differentiation curve and background understanding of the study area with six landcover classes namely, deciduous forest, bareland, water and marsh, floodplain and irrigation, shrubland and grassland and clouds. Supervised classification was used to classify the images.

The classification used the maximum likelihood classifier, an algorithm which assumes that spectral values of training pixels are statistically distributed according to a multivariate normal probability density function (Gumindoga et al., 2014b). Furthermore, the maximum likelihood decision is a methodology purely based on probability were other classifiers are principally centred on identifying decision borders in feature space using training class multispectral distance measurements (Jensen and Lulla, 1987).

To validate the classification output, a total of 207 GCPs (Figure 3-2) were collected in the study area by a GPS guided fieldwork according to the landcover classes. A point map was created in QGIS and exported to ILWIS. Using the Map Value function, the classified image

was added and computed together with coordinates. In SPSS, Cohen' Kappa was calculated to confirm the measure of agreement between the ground control points and the classified output.

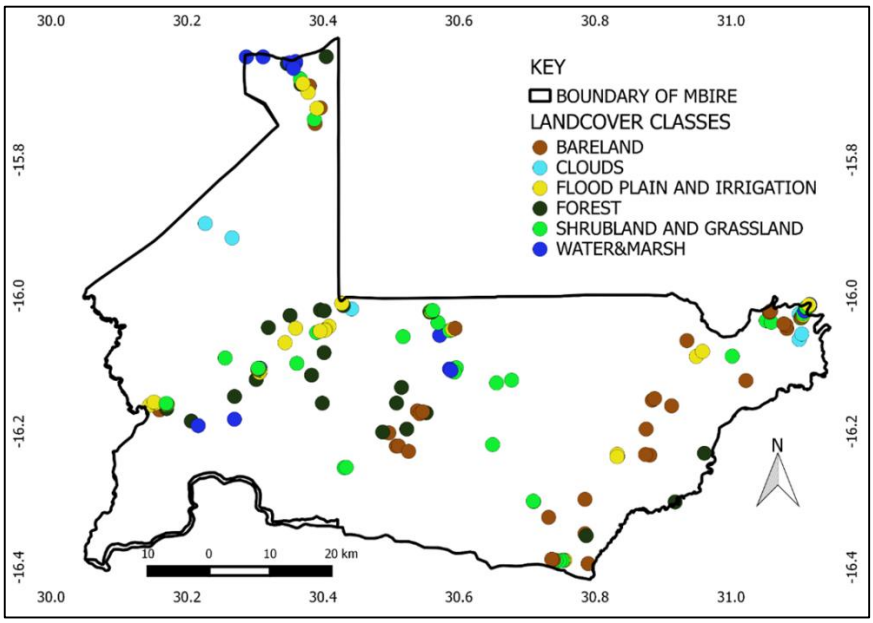

Figure 3-2: Ground control points for land classification

3.3.2 Generation of water and non-water random points

For each flood day, a total of 50 random points representing flooded areas and 50 random points representing non-flood areas were extracted from the MODIS data in order to generate flood presence flood absence data. The presence absence data was needed as input for the binary logistic regression were '1' represented water pixels and '0' represented non-water pixels.

The function (Equation 3) in ILWIS was used to retrieve elevation and other environmental variables including slope, TPI, landcover, soil type, distance from dams and distance from rivers that were deemed as important to explain the probability of flooding.

Equation 3

Vertical Channel Height= MapValue (Vertical Channel Height, Coordinate)

3.3.3 Estimating Probability of flooding

Binary Logistic Regression (Equation 4) is a type of stochastic model involving regression analysis where the dependent variable is a dummy variable (coded 0, 1). The regression equation is written as in Equation 4:

Equation 4

$$P = 1 / (1 + \exp (-1 * (b0 + x1 * b1 + x2 * b2 + \ldots. + xn * bn))$$

where b = the environmental constant

x = the factor map multiplied by the significant value ($p < 0.05$) of the factor

Data on the environmental covariates was opened in SPSS and testing for multi collinearity on covariates done to reduce redundancy. The Variance Inflation Factor test was carried out and those whose values were greater than 10 were eliminated. Regression was carried out and significant ($p<0.05$) factors and their days noted.

The spatial logistic function was applied to each derived variable map for each flood day in a GIS environment. Continuous probability maps indicating the probability of flood occurring were developed with maximum likelihood having a probability of 1 and least likelihood of flood occurrence having a probability of 0.

3.3.4 Development of flood hazard maps

Using the logistic equation in ILWIS, probability maps were produced and sliced into four flood hazard classes. The classes were chosen after a study by Gumindoga et al. (2014a) on the spatio-temporal variation of the 2014 floods in Tokwe-Mukosi as well as knowledge of study area. Histograms of the probability maps classes were used to determine the value ranges of the four hazard classes that are very low hazard, low hazard, high hazard and very high hazard. The values used for the classified flood probability maps are in Table 3.2

Table 3.2: Flood Hazard Classes

Hazard	Range
Very low hazard	<0.25
Low hazard	0.25-0.50
High hazard	0.5-0.75
Very high hazard	>0.75

3.4 Methodology for flood mapping using hydrological and hydraulic modeling techniques

This objective seeks to quantify the flows that leave the Mbire District and consequently determine the flows that affect flood magnitude in the district.

3.4.1 Hydrologic modelling through HEC-HMS

In this study, HEC-HMS a conceptual semi distributed physically based model developed for the rainfall-runoff simulation processes was used to simulate precipitation-runoff processes in three sub-basins. The model was chosen because of its capabilities in modeling a wide range of geographic expanses such as water supply, large river basin watershed runoff and flood hydrology. The model comprises of the open channel routing, losses, runoff transform rainfall-runoff simulations, parameter estimations and analysis of meteorological data. For each model run a combination of, a basin model, control specifications and meteorological model was done for each sub-basin.

HEC-HMS model used inputs such as soil type, evaporation, catchment area, lag time, precipitation, peaking coefficient and runoff coefficient to simulate flows. The runoff simulation process includes components such as direct runoff depth, channel routing and base-flow. The following methods were selected for the components based on data availability, applicability and limitations.

The transform method

The SCS Unit Hydrograph was selected in estimating direct runoff. Runoff depends on soil infiltration rates hence soil data was considered as an important factor in the model development. Soils helped to explain the loss method through their infiltration rates. The soils

were categorised according to the soil hydrologic grouping which indicates the minimum rate of infiltration acquired for bare soil after a lengthy wetting. According to Food and Agriculture Organization (2015) Group A soils comprise of low runoff potential and high infiltration rates when wetted. The soils are well drained sands with gravel of high rate of water transmission (> 7.62mm/hr).

Group B soils have a moderate infiltration rate and comprise of moderately coarse textures which are well drained. Their infiltration rate (2.54-7.62mm/hr) is moderate. Group C soils have a layer that hinders downward movement consist with low infiltration rates and fine textured soils. Their transmission rate is low (1.27-2.54 mm/hr). Group D soils are clays that have very high runoff potential and very low infiltration rates. The soils have a very low water transmission (0-1.27mm/hr).

The soils in the study area derived from the FAO soil classification show the predominant soil types based on the Hydrologic Soil Group Classification. The soil types are Ferralic Arenasols in Hydrological Soil Group B, Lithosols, Ferric Luvisols and Chromic Luvisols are in Hydrological Soil Group D.

Routing method

In this study, the Muskingum method for channel routing was chosen. In this method, X and K parameters were evaluated where the K parameter is estimated as the interval between similar points on the inflow and outflow hydrographs and X parameter is a constant coefficient with values from 0 to 0.5 (William et al., 2008).

The loss method: deficit and constant

The loss method calculated the rainfall losses absorbed into the ground and controls the partitioning of water that is intercepted-infiltrated and that water that leaves the catchment as direct runoff. The water that is not affected by a loss method leaves the catchment as quick flow (HEC, 2000). The Deficit and Constant model, a quasi-continuous model was chosen for the loss method for precipitation losses and used for continuous simulation. Empty storage

depth at the beginning of the simulation and constant rate was specified at hourly basis (Gumindoga, 2012).

Reservoir methods

The reservoirs were used to model the detention and attenuation of a hydrograph. The Specified-release method was chosen for the model because of its usefulness during calibration of the model and observed releases from the reservoirs will be known. For the storage, Elevation-Area-Outflow was selected and the elevation-area curves for each reservoir. The elevation-area relationship so that the storage-volume relationship of the reservoir can be computed (HEC, 2000).

Creating a basin model

To create the background map for the model, drainage network extraction and catchment extraction was carried out. In QGIS, extraction and clipping was carried out for each of the three subbasins, Angwa, Manyame and Musengezi from SRTM. The DEMs were exported to ILWIS for Hydroprocessing. The catchment map and other important shapefiles such as dams in ILWIS were exported as ArcView shapefiles. In the HMS interface, the shapefiles were imported as ÉSRI shapefiles.

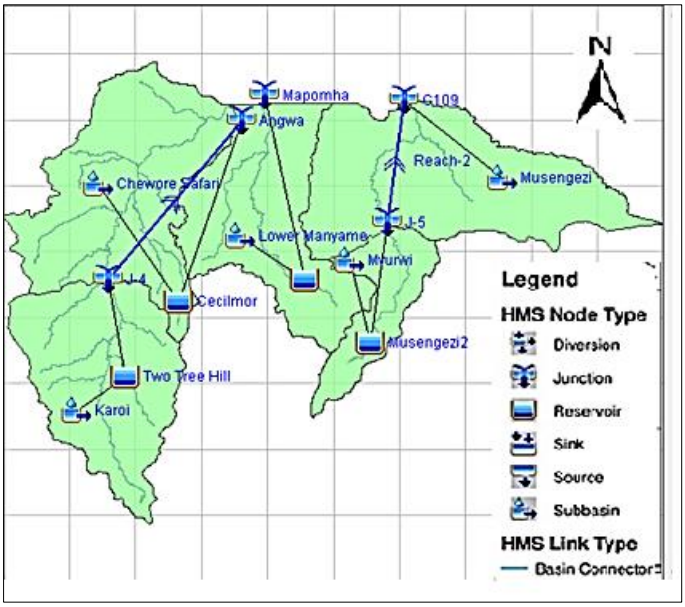

Figure 3-3: Model representation of watersheds in HEC-HMS

Hydrologic elements which include 5 subbasins, 2 reaches, 4 reservoirs, and 3 junctions were created (Figure 3-3). In defining the storage properties of the reservoirs, specified release

option and Elevation-Area-Outflow storage methods were chosen due to their useful roles when calibrating a model and observed releases from the reservoir are known. The specified elevation-area relationship was chosen because it is the one used to compute the storage-volume relationship of the reservoirs.

Developing a meteorological model

Data types needed for the meteorological model are rainfall, average monthly evaporation and the gauge weights of the different weather stations. The weather data was acquired from 8 weather stations namely, Kanyemba, Rukomechi, Karoi, Mushumbi, Guruve, Mvurwi, Mt Darwin and Muzarabani. Thiessen polygons were developed from a point map to determine the spatial distribution of rainfall in the 5 subbasins and also determining the gauge weights of each rainfall station. A point map was created in QGIS and exported to ArcGIS where the Thiessen polygons were created from the point input features (Figure 3-4) and Table 3.3 shows the thiessen weights. The rainfall characteristics as determined by the Thiessen polygons are different within a polygon so rainfall analysis took into account the shortfall in representativeness.

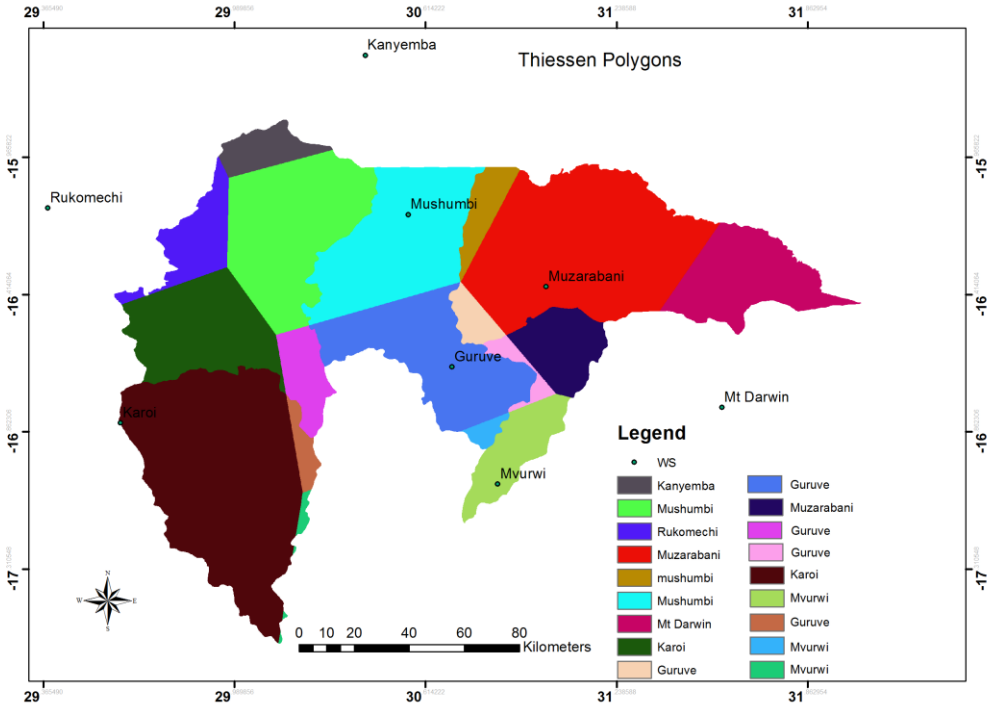

Figure 3-4: Thiessen Polygons for Angwa, Lower Manyame, Mvurwi, Karoi and Musengezi subbasins

Table 3.3: Thiessen weights for HEC-HMS model

Subbasin		Area(km^2)	Total Area	Thiessen weight	Total Weight
Angwa	Rukomechi	652.1715		0.124225897	
	Kanyemba	405.4437		0.077229084	
	Karoi	1542.2355		0.293765656	
	Mushumbi	2177.829		0.414833769	
	Guruve	472.2039	5249.8836	0.089945594	1
Karoi	Karoi	3959.4654		0.945977804	
	Guruve	174.8448		0.041773139	
	Mvurwi	51.2694	4185.5796	0.012249056	1
Lower Manyame	Mushumbi	2091.0123		0.518425107	
	Guruve	1845.5733		0.457573365	
	Mvurwi	96.8076	4033.3932	0.024001528	1
Musengezi	Mushumbi	353.6856		0.06532101	
	Guruve	225.6723		0.041678662	
	Muzarabani	3518.5617		0.649831388	1
	Mt Darwin	1316.6568	5414.5764	0.243168939	
Mvurwi	Guruve	147.582		0.095967919	
	Mvurwi	688.6188		0.447787084	
	Muzarabani	701.6256	1537.8264	0.456244996	1

The meteorological model stores the precipitation and evapotranspiration data used in simulating a watershed. The model was used to represent rainfall in the form of a storm hyetograph and the start time as well as end time was defined. Average annual precipitation depths were interpolated using the Thiessen polygons which were used to specify indices for storm gages for each sub-basin and weather station.

Calibration and validation

The available hydro-meteorological data at Angwa station in Angwa basin, C109 station in Musengezi and Mapomha station in Lower Manyame was split in two for model calibration and for model validation, data from October 2004 to September 2008 was used in calibration and October 2008 to September 2009 was used for validation since it corresponds to 2008-2009 flood year. The simulations did not consider the contribution of a different upstream catchment including Harare, Marondera because of data which is not good as well as presence of a lot of private owned dams.

The success of the hydrologic simulation model depended on how well the model was calibrated and the quality of the input data (Heimhuber, 2013). The objective of calibrating was to match the observed simulated runoff flows against the runoff peaks and timing of hydrographs with the observed ones. The parameter values essential for calibration were calculated and given as initial values at the time of calibration to the selected model.

Single-response and multi-response efficiency measures were used to provide an unbiased assessment of the closeness of the simulated behaviour to the observed measurements. The Nash-Sutcliffe Efficiency (NSE) is a standardised statistic used to define the relative degree of the residual variance ("noise") compared to the measured data variance ("information") (Nash and Sutcliffe, 1970). The NSE was used in the study to show how well the observed plot against simulated data fits the 1:1 line. NSE values range between $-\infty$ and 1.0 (1 inclusive), with NSE = 1 being the ideal value. Positive values in the range of 0.0 to 1.0 are regarded as suitable levels of performance, and negative values indicate that the mean observed value is a better predictor than the simulated value, which indicates unacceptable performance of the model (Moriasi et al., 2007).

The Nash-Sutcliffe Index (Equation 5) was used to determine the goodness of fit of the simulated to the observed values.

Equation 5

$$E = 1 - \frac{\sum_{t=1}^{T} (Q_0^t - Q_m^t)^2}{\sum_{t=1}^{T} (Q_0^t - \overline{Qo})^2}$$

where Q_o = observed flow in m^3/s

Q_m = simulated flow in m^3/s

Other statistical measures were evaluated at each of the gauged stations to assess the performance of the model that include the measure of the relative bias (RBIAS) and relative root mean square error (RRMSE). The RBIAS (Equation 6) compares the simulated and the observed flows. Values close to zero show a very good model simulation though up to 10% are still acceptable.

Equation 6

$$RBIAS = 100* \frac{1}{N} \sum_{t=1}^{N} \left(\frac{Qm-Qo}{Qo}\right)$$

where Q_m = simulated flow in m^3/s

Q_o = observed flow in m^3/s

The Relative Root Mean Square Error is based on the standard root mean square error. By taking the square root of the mean square error, the error to the quantities being predicted are reduced. The RRMSE values range from 0 to infinity with values close to zero most ideal. Measure of relative root mean square error in Equation 7 was also used.

Equation 7

$$RRMSE = 100* \sqrt{\left(\frac{1}{N} \sum_{t=1}^{N} \left(\frac{Qm-Qo}{Qo} \right) \right)}$$

3.4.2 Flood routing through HEC-RAS

The hydraulic model, HEC-RAS was used to outline the positions of the waterway in places where bank overtopping is most likely to occur after a certain threshold flood flow is exceeded. The model setup in HEC-HMS was modified to cater for Lower Manyame Catchment only because that is where the most significant floods occur as well as the data available in Lower Manyame was sufficient for the model simulations. Lower Manyame Catchment was further subdivided into three sub-basins using the DEM Hydroprocessing technique. Figure 3-5 is a schematic of the modified Lower Manyame in HEC-HMS.

HEC-HMS model simulation was carried out for the hydrological periods between 1 October 2004 and 30 September 2012. Calibration was carried out changing the Muskingum K and X values as well as the infiltration rates.

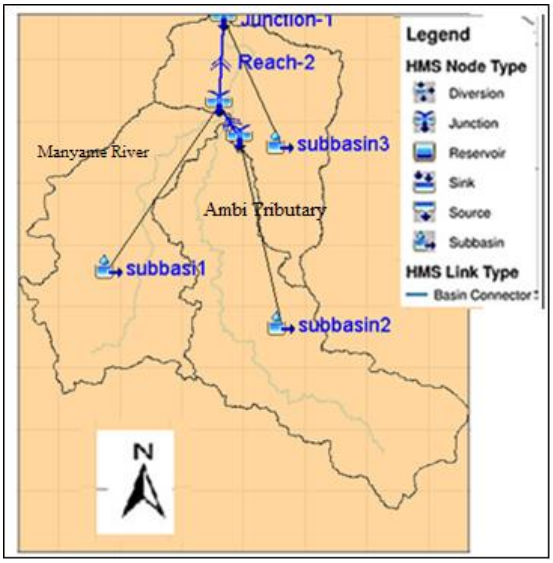

Figure 3-5: Model representation of Lower Manyame Catchment in HEC-HMS

Model extend and DEM selection

The model geometry was developed displaying the areas significant for the flood hazard analysis and selecting the topographic dataset for the model development (Pappenberger et al., 2005). Since no previous flood risk analysis for the region had been done, the model had to start sufficiently upstream in order to deliver accurate results for Lower Manyame. The downstream end of the model is where the catchment enters into Mozambique. The total length of the modelled reaches between the up-and downstream end as well as the corresponding sub basins areas are shown in Table 3-4.

Table 3.4: Reach lengths in HEC-HMS

Reach	**Length (m)**	**Catchment Area (m^2)**
Upstream (Manyame)	35703	1144.1
Downstream(Manyame)	33375	851.6
Tributary (Ambi)	34309	1477.8

Digitizing of the flow lines, which are the floodplain extent lines, banks, which are the edges of the river, the river centre line and cross sections was done in QGIS through the Bing Aerial plugin. The Lower Manyame DEM was used in QGIS to calculate 30 m contours.

Data pre-processing

Contours created in QGIS defined elevations which were used to create a triangular irregular network (TIN) in ArcView using 3D Analyst tool and AVRas 1.2 HEC-RAS extensions. The TIN contains terrain information which is used to generate a geometry file that can be read by HEC-RAS (Knebl et al., 2005). Digitizing of different input layers defining the banks, stream centreline, cross sections and flowlines was carried out following important rules in QGIS. The bank lines, flowlines, centrelines and cross lines had to start from upstream going downstream. Special attention was put on the placement of the cross sectional cutlines in the geometric model development. The following data quality checks were considered for the placing of the cross section cut lines according to HEC (2010b).

Cross sections were drawn at representative positions along the modeled reaches at locations where changes in slope, shape, discharge or roughness happened. Cross sections were drawn from the left bank to the right bank thus spanning across the flow network and the entire floodplains. The cross sections were placed perpendicular to the flow paths in the channel. In the model development, the cross sections assumed to represent the channel geometry half way to the next up- and downstream cross section (HEC, 2009). The spacing of the cross-section lines along the modeled reach depended on the channel size and slope as well as on the uniformity of the cross section shape (Azagra and Olivera, 1999).

Since the positioning of the cross sections have a direct effect on the model accuracy and stability, equations have been developed to estimate the maximum cross section spacing as a function of different channel factors. HEC (2010b) proposed the use of Equation 8 which delineates the maximum distance between cross sections based on the average bank full depth of the main channel (D) and the average channel bed slope S_o.

Equation 8

$$\Delta X \leq \frac{0.15D}{So}$$

where D = channel depth (m)

S_o = channel bed slope (%)

The overbank flow paths were drawn parallel to the stream centreline at a constant distance away from the channel banks. The themes were imported into ArcView and based on the subsequent layers, cross sectional elevation data was extracted from the DEMs while cross-sectional properties were defined based on points of intersection of the digitized layers (Brunner, 2008). The resulting data was automatically generated to a RAS-GIS export file, which was then imported in HEC-RAS. Figure 3-6 gives an overview of the geometric model configuration in ArcView for the Lower Manyame Catchment.

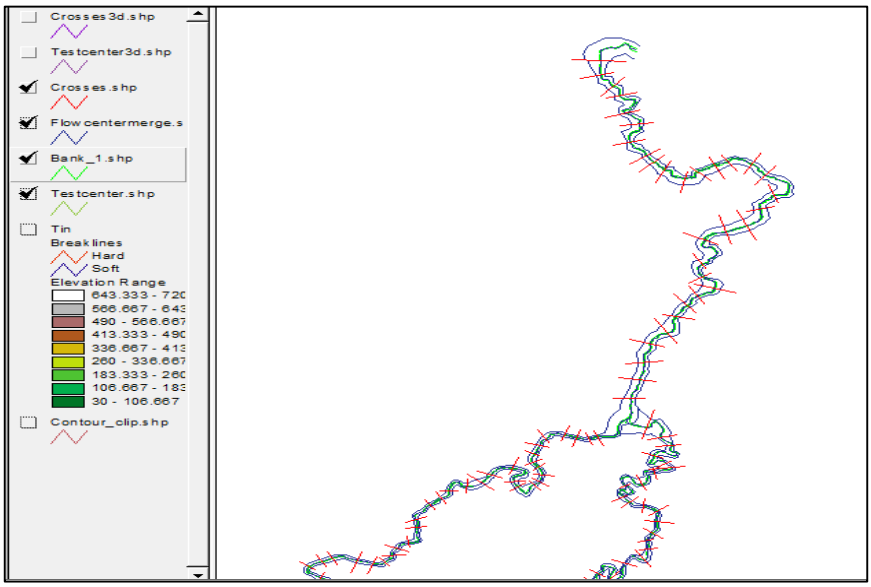

Figure 3-6: Schematic view of flowlines, crosssections, centreline and bank lines

Model setup in HEC-RAS

In HEC-RAS, the GIS format data was imported showing the files created during pre-processing in ArcView, the geometric data view presented in Figure 3-7. The methodology for the definition of the *Manning´s* roughness coefficient for the catchments flow channel used the figures from the T-R 55 methodology table (NRCS, 1986) in Appendix C 1.

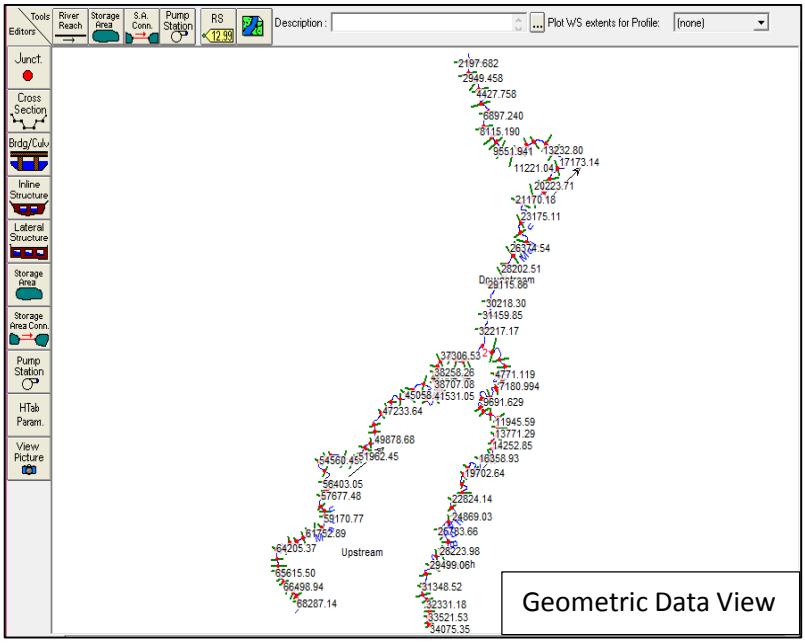

Figure 3-7: Geometric data view in HEC-RAS

The Manning roughness coefficient ranges from 0.011 for smooth surfaces, such as concrete, to 0.8 for forests with dense underbrush (Cameron and Ackerman, 2009). For the study, the coefficient was defined as 0.04 for both banks which corresponds to the roughness of a short grass, bare land and cultivated soils. The selection was based on field observation as well as Google Earth images. The main channel was assigned a roughness coefficient of 0.03. The roughness n coefficient of the channel overbank areas is usually higher than for the channel owing to the presence of obstructions such as trees or houses thus for the overbanks, 0.04 was selected.

Flow Data and Boundary Conditions

Boundary conditions for steady-flow simulations were defined for the beginning and end of the model (Brunner, 2010). If the flood hydrograph at the downstream end of the modeled reach is unknown, as it was the case in this study, the normal depth was used instead as the downstream boundary condition.

Thus the water level at the last cross section was calculated for a friction slope by using the Manning´s equation. The friction slope was not known and it was estimated as the channel bed slope in the area of the last cross section (Warner et al., 2010). This method involved high levels of uncertainty hence the last cross section cutline was placed downstream of where the bottleneck of the channel was expected.

For the estimation of different flood return flows, the Gumbel distribution stochastic model was used. The Gumbel extreme value distribution was used to analyse variables including annual maximum values of daily river discharge volumes. The distribution is commonly applied in flood frequency analysis involving fitting of a probability model to the sample of annual flood peaks recorded over a period of observation for a catchment (Mujere, 2011b). The data available for the model was for 8 years. The distribution was chosen because it caters for data less than ten years as well as incorporating annual exceedance on flood series data selection.

As highlighted in Chapter 2, probability distributions are based on averages and standard deviations of data. The flood series data from October 2004 to September 2012 was assembled and the peak annual flows identified. The mean ($\bar{x}$) of the peak flood discharges for the years was calculated as well as the standard deviation (s). The average flows for the record period ($\bar{y}$) for the record period and the standard deviation (σ_n) was determined as a function of record length *n* from the Gumbel distribution table where *n* was 8 years from the number of years of data.

Several return periods were selected, 10 year, 25 year, 50 year and 100 year these were associated with the exceedance probability P_j. Equation 9 was used to calculate Gumbel variate y corresponding to return period T.

Equation 9

$$y = -\ln\ln \frac{T}{T-1}$$

where y = Gumbel variate

T = return period (years)

The flood discharge (x) for each Gumbel variate and associated return period was computed using equation 10.

Equation 10

$$x = \bar{x} + \frac{y - \bar{y}}{\sigma} s$$

where x = flood discharge (m^3/s)

$\bar{x}$ = mean peak flow (m^3/s)

s = standard deviation,

y = Gumbel variate,

$\bar{y}$ and σ are the mean and standard deviation for the Gumbel variate respectively.

The reach boundaries were assigned and the downstream energy slope was set at 0.001 using normal depth as highlighted earlier. The model was executed using FORTRAN based program called SNET which carries out the computations (Brunner, 2008).The data was exported as a GIS Data file.

Post processing in a GIS environment and validation

The water surface elevations were computed in AVRas. A TIN was created with the water surface elevations and compared to the terrain TIN created during pre-processing in AVRas in defining the flooded areas (Cameron and Ackerman, 2009). The technique converts the flooded areas into a polygon theme thus forming the floodplain theme. The validation of the HEC-RAS flood inundated areas was done using 39 GCPs collected in the field using GIS participatory mapping and GPS. The control points were collected on the 24th of December 2015 in Mushumbi Pools, Chikafa and along Dande River (downstream of Manyame River).

A point map with the GCPs was created in QGIS and overlayed by the flood water surface profile maps from HEC-RAS model in ILWIS. Since no current (2013-2015) flow data is available, validation was done using the 2008-2009 flood. Results in an ILWIS table format were exported to SPSS. In SPSS analysis tests were carried out to measure the agreement of the ground control points and the HEC-RAS derived flooded area. Measure of agreement was first carried out using the Cohen Kappa Test.

CHAPTER FOUR: RESULTS AND DISCUSSION

4.1 Variation of flood inundated areas

Figure 4-1 shows the MODIS NDVI derived maps for flood presence and flood absence for the different days. The results show that 16 January had the largest area inundated for the season 2005-2006 (1934 km^2). The inundated areas covered Chidodo, Musengezi, Muzeza, Mushumbi and parts of Angwa which are mostly settled areas. The areas as shown are close to catchment outlets along Manyame River, Musengezi River and Angwa River.

The 2008-2009 season saw 7 January 2009 having the most inundated area of 1225 km^2 in areas close to catchment outlets. The 17 December 2008 flood inundated area covered much of the northern part which is Kanyemba. Kanyemba is situated very close to the Zambezi River. The second largest inundated area was captured on 19 January 2009 covering 847 km^2.

Flood inundated areas for the hydrological season 2013-2014 had the highest area covered with water at time of image acquisition on 1 January 2014 of 1158 km^2. The areas covered were Kanyemba, Angwa, Mushumbi Pools, Chikafa and Chidodo. The areas as seen are close to river networks as well as to the catchment outlets. The second largest area was 765 km^2 on 13 December 2013 covering Angwa and parts of Kanyemba.

For the 2014-2015 season, 8 January had the largest area of 1895 km^2 flooded at the time of image acquisition. The whole of Kanyemba, Hunyani, and Chikafa were flooded at the time of image acquisition.

It can be noted that the areas frequently flooded are Kanyemba, Chikafa, Hunyani and Chidodo. These areas are situated very close to catchment outlets. Figure 4-1 shows the areas mapped as floods in the Mbire District from 2005-2006, 2008-2009, 2013-2014 and 2014-2015 hydrological seasons.

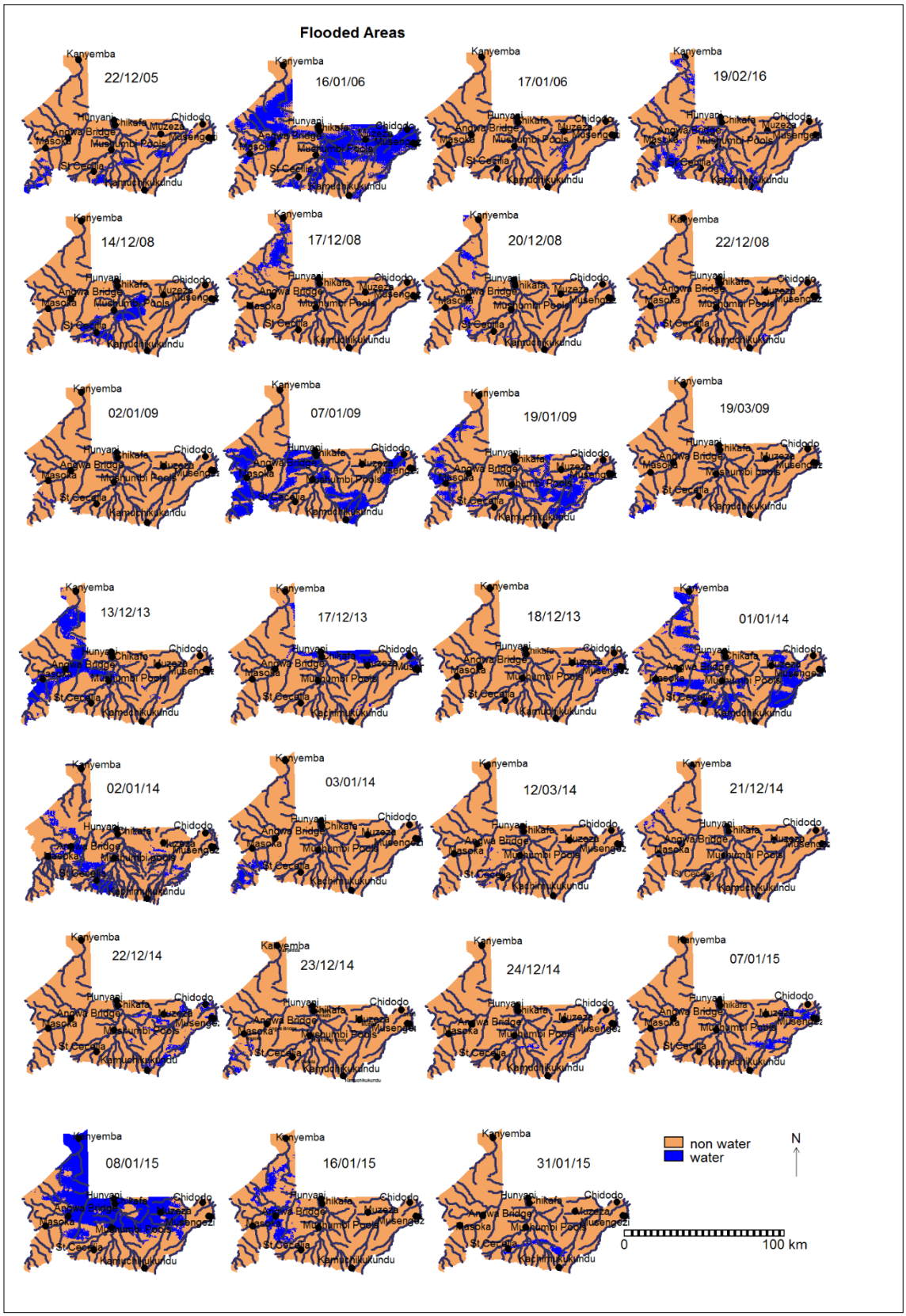

Figure 4-1: The spatial and temporal variation of flooding for the seasons between 2005 and 2015

Table 4.1 gives a detailed summary of all the flood inundated areas as captured by the satellite at the time of image acquisition. From Table 4.1 it can be seen that of the selected seasons, the 2005-2006 hydrological season had the greatest area inundated of 1934 km^2 according to the satellite image. The 2014-2015 season had second highest area of 1895 km^2 followed by the 2008-2009 season. It can also be noted that the maximum areas exceed 1000 km^2 in all flood events.

Table 4.1: Area flooded in Mbire District for hydrological seasons, 2005-6, 2008-9, 2013-14 and 2014-15

DATE	AREA INUNDATED (km^2)
22 December 2005	317
16 January 2006	1934
17 January 2006	51
19 February 2006	432
14 December 2008	313
17 December 2008	221
20 December 2008	121
22 December 2008	40
2 January 2009	20
7 January 2009	1225
19 January 2009	847
19 March 2009	41
13 December 2013	765
17 December 2013	306
18 December 2013	79
1 January 2014	1158
2 January 2014	482
3 January 2014	139
12 March 2014	37
21 December 2014	26
22 December 2014	232
23 December 2014	58
24 December 2014	36
7 January 2015	195
8 January 2015	1895
16 January 2015	370
31 January 2015	110

4.1.1 Validation of MODIS derived flood areas

Validation of the MODIS derived flood images was done using 68 GCPs collected using GIS participatory mapping method. The statistical analysis was done on the MODIS flood image of January 8 2015 and the ground control points.

A point map was created in QGis and the shapefile created was imported into ILWIS. Using the "MapValue" function, the January 8 flood presence and flood absence map was added. After analysis in SPSS, the results show a substantial measure of agreement between the GCPs and the MODIS derived flooded area. The Area Under Curve (AUC) results showed a significant measure of agreement ($p<0.05$) between the ground points and MODIS flood evidence of 0.86.

Cohen's KAPPA, showed a significant measure of agreement ($p<0.05$) of 0.69. Hence confirming the applicability of the methods used in calculating the inundated areas for Mbire District. The results show that areas frequently flooded are Chidodo, Musengezi, Angwa, Chikafa and Mushumbi Pools. These results are helpful to managers and communities to better prepare themselves for flood events or better cope with the events.

4.2 Factors affecting flood magnitude

4.2.1 Environmental factors

In coming up with factors affecting flood magnitude, temporal and static factors were considered. Figure 4-2 shows the environmental factors used in the model.

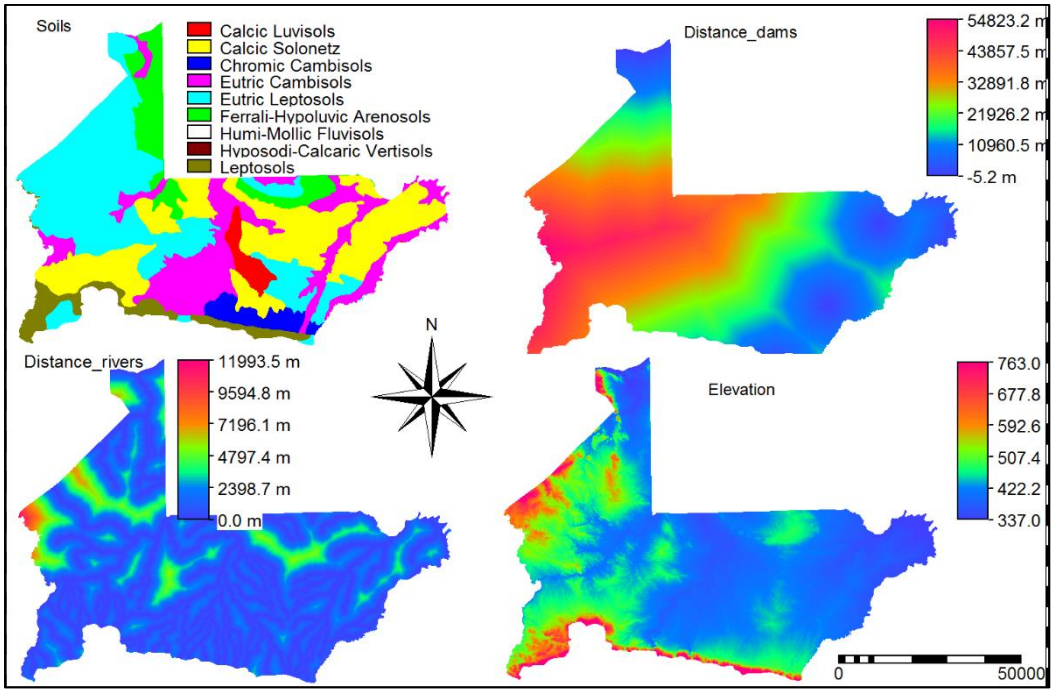

Figure 4-2: Environmental inputs

Landcover

Figure 4-3 shows classified land cover change maps for Mbire District. Using the supervised image classification of 2005, 2008, 2013, 2014 the following landcover classes were used; Bareland, Shrubland and grassland, Water and Marsh, Deciduous forest, clouds and floodplain and irrigation.

Validation of the landcover classification

Validation of the landcover classification output was carried out in SPSS using Cohen' Kappa. In ILWIS, the point map of the 207 GCPs collected between 24 and 25 December 2015 was combined with the classified output of September 2014. The table was imported in SPSS and tested for agreement. A significant measure of agreement ($p<0.05$) of 0.71 between the GCPs and the classified output was computed using Cohen Kappa.

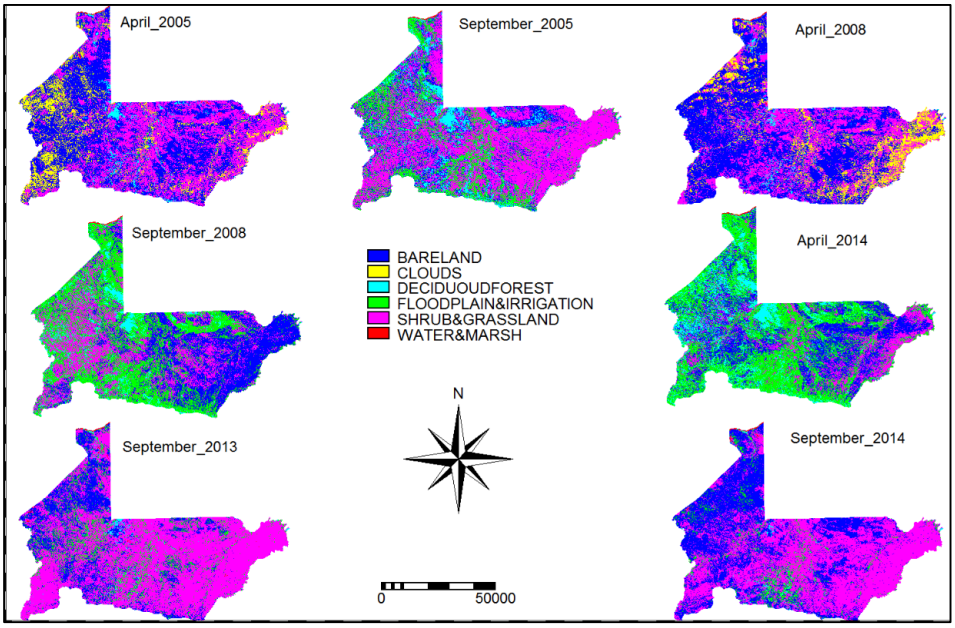

Figure 4-3: Landcover maps for April and September

4.2.2 Flooding condition and environmental variables

Environmental factors control the movement of flows, flows which then affect the magnitude of floods. After failing to establish satisfactory temporal dynamic variables, static variables were used for this study.

Relationship between flooding and distance from dams

Table 4.2 shows the relationship between the probability of occurrence of flooding and distance from dams (DD) in and around Mbire District, with Cahora Bassa as the biggest dam. The results show a significant relationship ($p<0.05$) between distance from dams and probability of occurrence of variation of flooding based on data from one day. A study by Zhang et al. (2015) in East River Basin , China concluded that Xinfenngjiang reservoir has a significant influence in flooding near Heyuan station. This shows that distance from dams can explain why flooding occurs in Mbire District. Figure 4-4 is a graph that shows decrease in probability of flooding with increase in distance from reservoirs.

Table 4.2: The relationship between distance from dam and presence and absence data for flooding

Date	Variables	B	Sig.	Equation
22/12/05	Distance_dams	0.000099	**0.040**	P=exp(-16.519+0.000099*DD)/(1+exp(-16.519+0.000099*
	Constant	-16.519	**0.018**	DD))

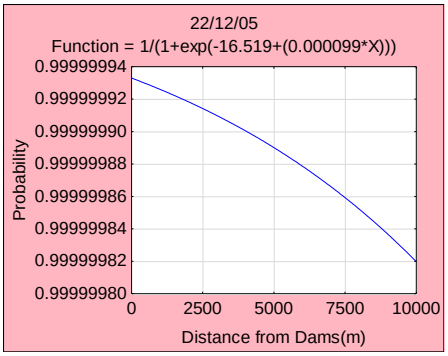

Figure 4-4: Probability of flooding explained by distance from dams

Table 4.3 shows the variation of flooding with distance from the river network (DR) in Mbire District where 2 days show a significant relationship between flooding and distance from rivers. Murwira and Schmidt-Murwira (2005) considered distance from river networks when they prepared a Flood Warning System for Muzarabani as one of the factors that explain flooding in the area. The graphs in Figure 4-5 show that the probability of flooding decreases with increase in distance from river networks.

Table 4.3: The relationship between distance from rivers and presence and absence data for flooding

Date	Variables	B	Sig.	Equation
22/12/05	Distance_rivers	0.001	**0.027**	P=exp(-9.035+0.001* DR)/(1+exp(-9.035+0.001* DR))
	Constant	-9.035	**0.023**	
02/01/09	Distance_rivers	0.001	**0.013**	P=exp(-16.597+0.001* DR)/(1+exp(-16.597+0.001* DR))
	Constant	-16.597	**0.002**	

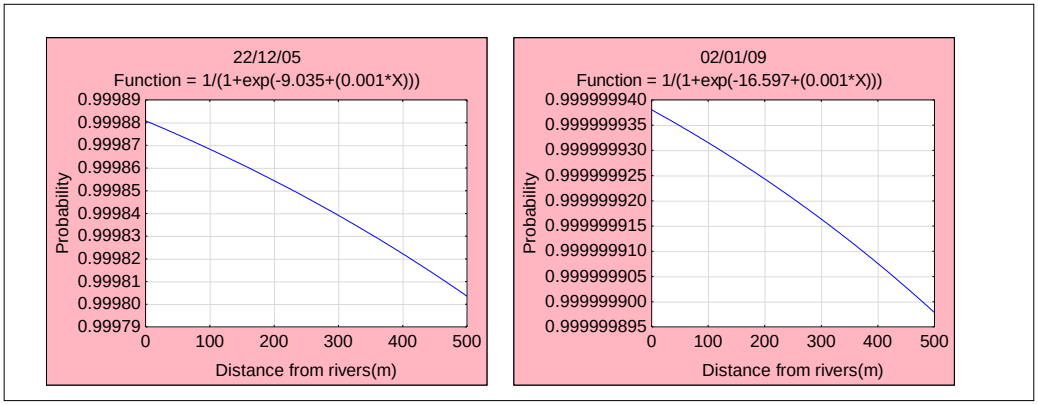

Figure 4-5: Probability of flooding explained by distance from rivers

The probability of flooding with variation in distance from rivers is shown in Figure 4-6. It can be shown that the probability of flooding is very high in and close to river networks.in most places (more than 0.6). The probability of flooding increases close to the rivers hence areas close to rivers are susceptible to flooding. Any developments in the district should not be close to the river network as these areas are at risk of flooding.

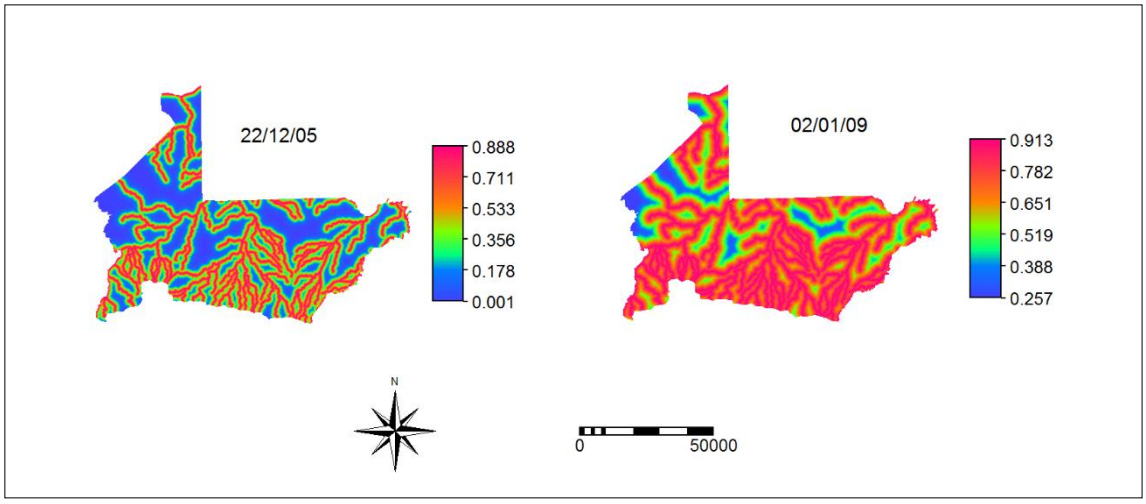

Figure 4-6: Probability of flooding with variation in distance from river networks

Figure 4-7 shows the flood hazard maps developed as a function of distance from rivers. From the maps it can be appreciated that areas close to the stream networks are at high risk of flood and inundation hazard.

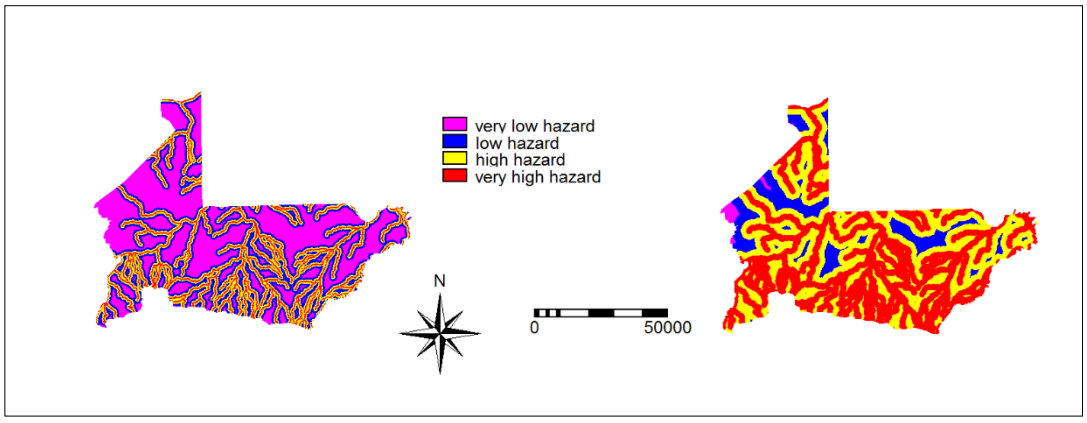

Figure 4-7: Flood hazard as a function of distance from rivers

Landcover and soils

A linear relationship between class and value data could not be fit hence failure to explain the relationship between landcover and probability of flooding as well as soil classes and probability. However further studies that can incorporate class data need to be pursued. There were no significant flood days explained by vertical channel height.

4.3 Hydrological modeling for flood mapping in the Mbire District.

4.3.1 HEC-HMS Model Calibration and Validation

In this section, the hydrographs resulting from hydrologic modeling of two periods, 1 October 2004 to 30 September 2008 and 1 October 2008 to 30 September 2009 are shown.

Model calibration

Initial simulation of the model was done for the years, 1 October 2004 to 30 September 2008. The model performance was done during calibration for the three catchments, Musengezi (C109), Lower Manyame (Mapomha), Angwa (Angwa). Table 4.4 shows the average annual outflows recorded against observed flows at the three stations. It can be observed that for Lower Manyame Catchment the model simulated flows close to the observed flows. Angwa model overestimated the flows with a simulated flow of $20.7 * 10^7$ m^3/year against an observed flow of $12.9 * 10^7$ m^3/year.

Table 4.4: Calibration model simulation outflow and observed flows

CATCHMENT(STATION)	OUTFLOW (m^3/annum)	OBSERVED (m^3/annum)
Musengezi (C109)	$20.0 * 10^7$	$24.9 * 10^7$
Lower Manyame(Mapomha)	$18.5 * 10^7$	$18.4 * 10^7$
Angwa (Angwa)	$20.7 * 10^7$	$12.9 * 10^7$

Figure 4-8 shows the hydrograph for the calibration period for Musengezi Catchment. The Nash-Sutcliffe for Musengezi Catchment was 0.34, the RBIAS of -0.01 % and RRMSE of 0.51 %. These results confirmed the capability of the model to simulate the catchment response. The hydrograph shows that the model initially overestimates discharge from the

catchment by simulating discharge when there is no discharge resulting in high runoff. The model later simulates almost the same discharge seen with some peaks corresponding to the observed peaks.

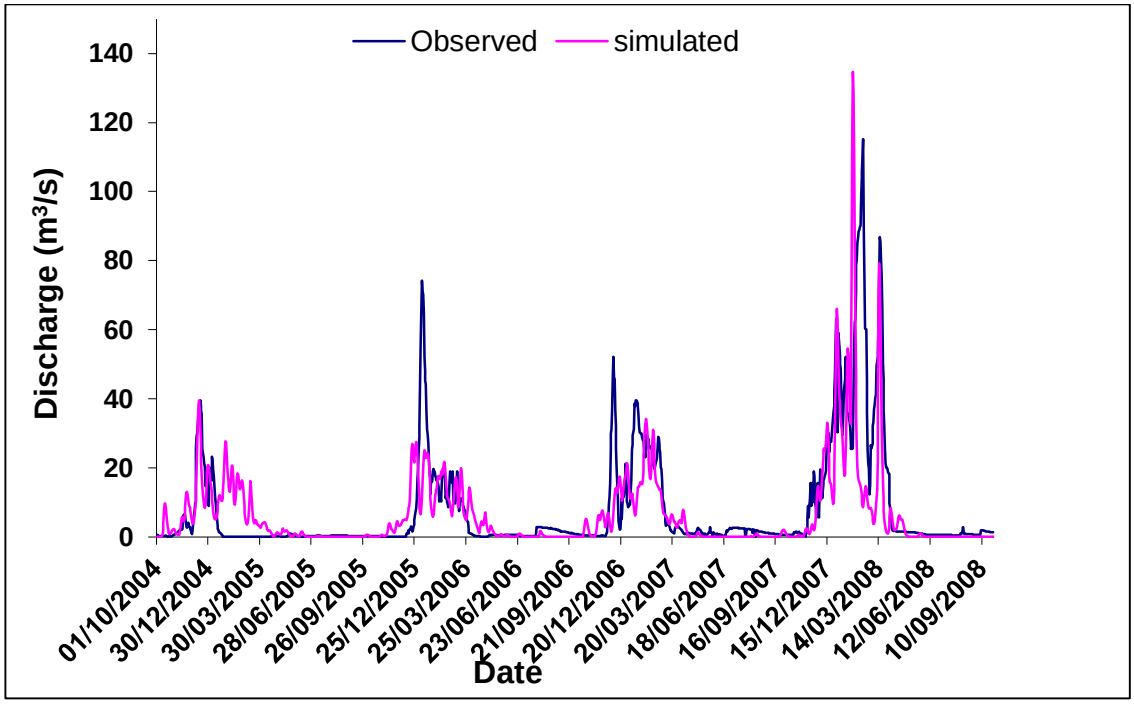

Figure 4-8: Calibration hydrograph for Musengezi Catchment

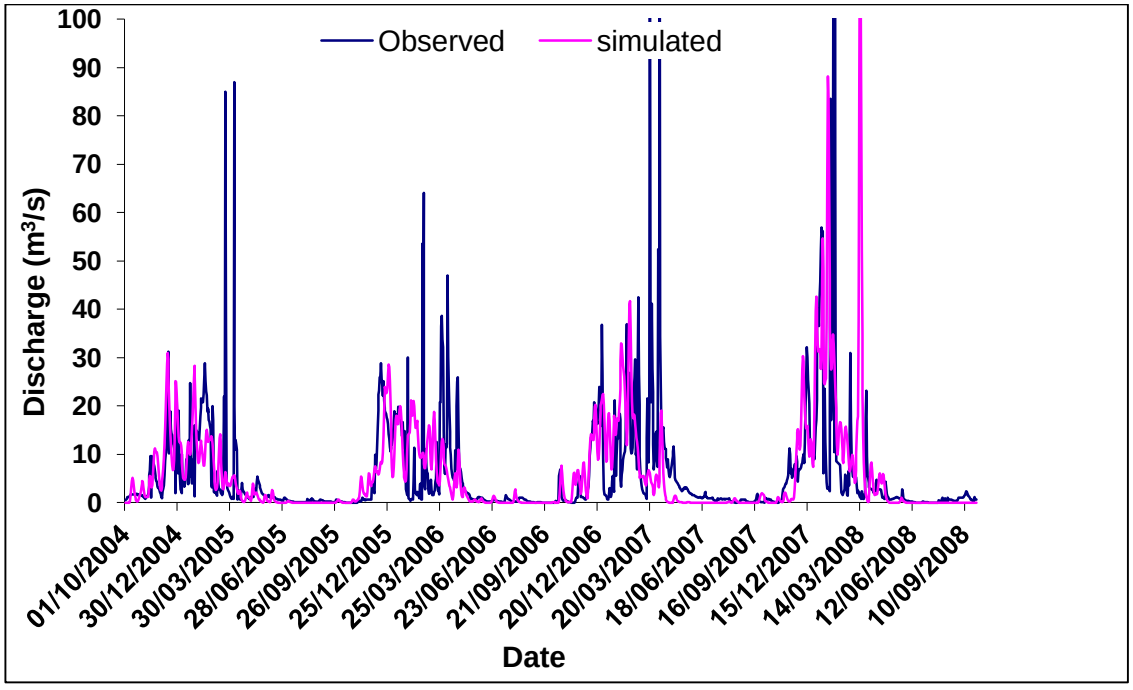

Figure 4-9: Calibration hydrograph for Lower Manyame Catchment

The NSE coefficient for lower Manyame Catchment (Figure 4-9) was -0.107 showing that the observed average is a better predictor of the discharge from the catchment than the simulated mean despite the low RBIAS of 0.001 % and RRMSE of 0.02 %. From the hydrograph, it is shown that the model simulates well in synch with the observed though underestimating some observed peaks. The peaks could be a contribution of rainfall which exaggerates outflow values (Czigany et al., 2010), erroneous flow data or upstream catchment contributions and private dam operations.

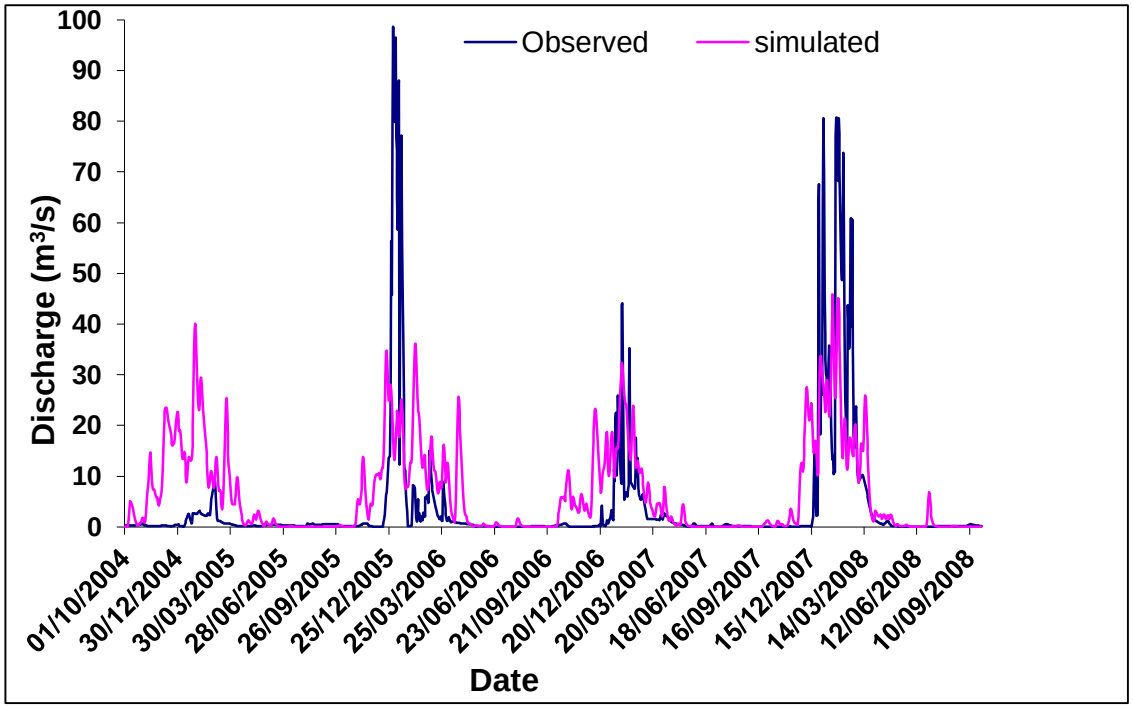

Figure 4-10: Calibration hydrographs for Angwa Catchment

The Nash-Sutcliffe coefficient for Angwa Catchment was 0.19, the RBIAS of -0.04 % and RRMSE of 1.59 % confirm the capability of the model to simulate the catchment response. The hydrograph shown in Figure 4-10 show how the model over-estimates the discharge for the period 2004-2005 and for the rest of the years underestimates. The peaks especially 2005-2006, floods occurred which might have been flash floods and the rainfall received exaggerates the observed flows (Czigany et al., 2010). The peaks could also be contribution from upstream catchment and dam operations where the control is limited. Table 4.5 gives a summary for model performances.

Table 4.5: Summary of the model performances during calibration for the catchments

CATCHMENT(STATION)	NSE	RBIAS (%)	RRMSE (%)
Musengezi (C109)	0.337	-0.013	0.510
L. Manyame(Mapomha)	-0.107	0.001	0.020
Angwa (Angwa)	0.188	0.041	1.581

Model Validation

Model validation was done after calibration with flow data from one hydrological season 2008-2009. Table 4.6 shows the validation cumulative outflows for that hydrological season and the observed outflows for the catchments.

Table 4.6: Validation outflows and observed flows for 2008-2009

CATCHMENT(STATION)	OUTFLOW (m^3/annum)	OBSERVED (m^3/annum)
Musengezi (C109)	$18.3 * 10^7$	$16.2 * 10^7$
Lower Manyame(Mapomha)	$19.7 * 10^7$	$15.6 * 10^7$
Angwa (Angwa)	$25.4 * 10^7$	$25.7 * 10^7$

Validation for Musengezi Catchment (Figure 4-11) had an improved NSE of 0.361 indicating a model performance that was acceptable further confirmed by the RBIAS of 0.036 % within acceptable ranges. However, the model peaks are out of synch this could be a contribution of a number of private dams in the catchment which are individually operated.

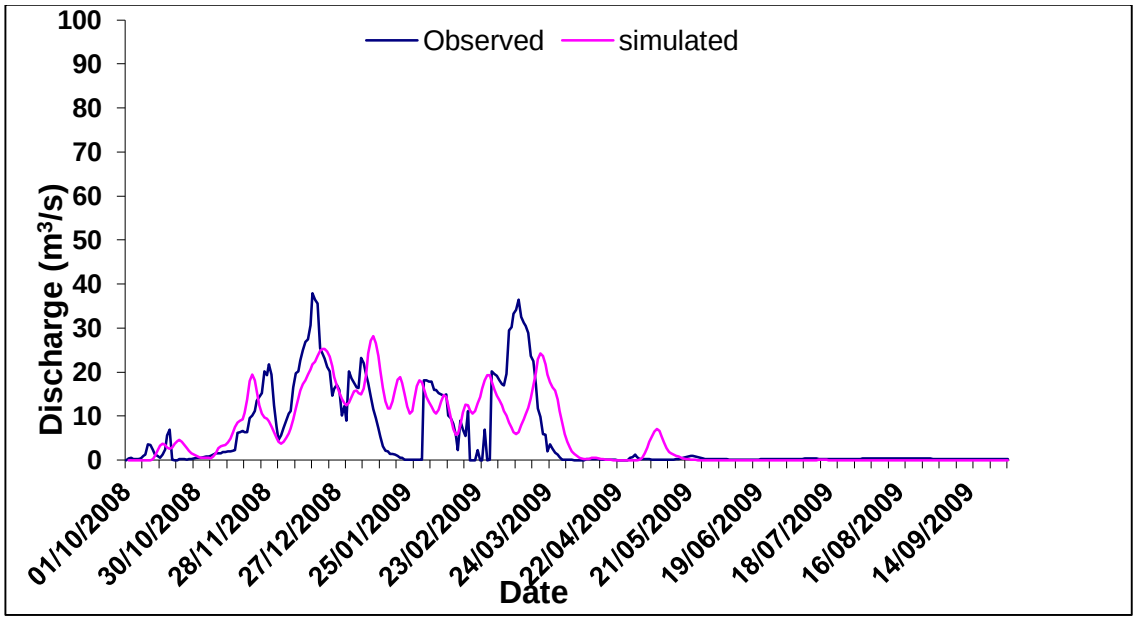

Figure 4-11: Validation for Musengezi Catchment

Model validation in the Lower Manyame Catchment (Figure 4-12), had an improved NSE coefficient of -0.008 and a RBIAS of 0.071 % still indicating that the observed mean is a better predictor of flow than the modeled mean despite the acceptable RBIAS. Two observed peaks were not simulated by the model this could be explained by the type of data used or rainfall received that period since a flood occurred which might have been a flash flood and hence exaggerated the flows (Czigany et al., 2010).

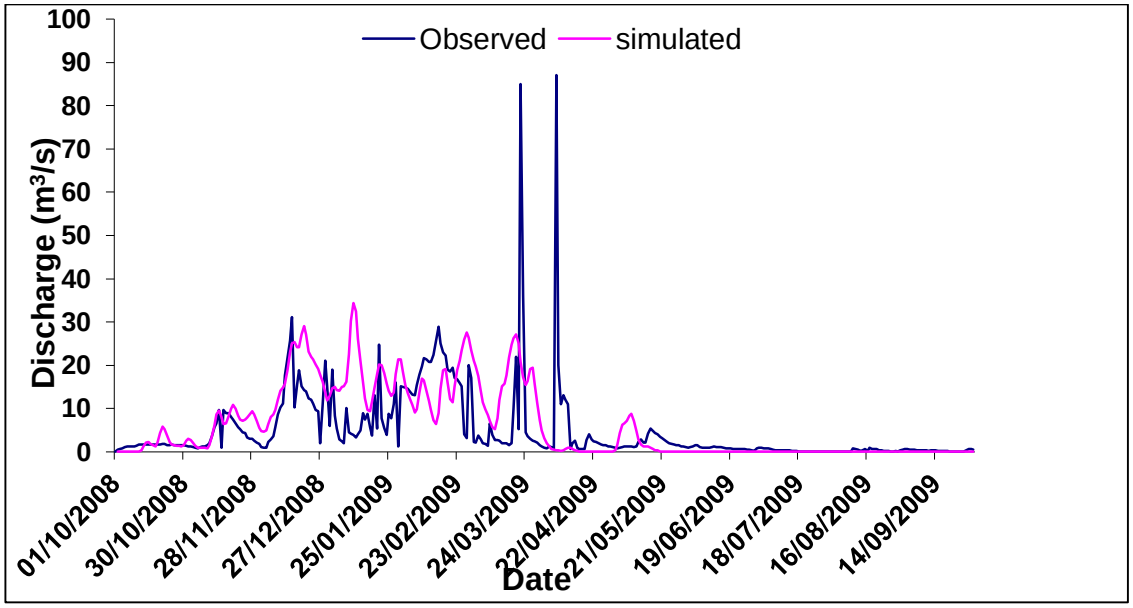

Figure 4-12: Validation for Manyame Catchment

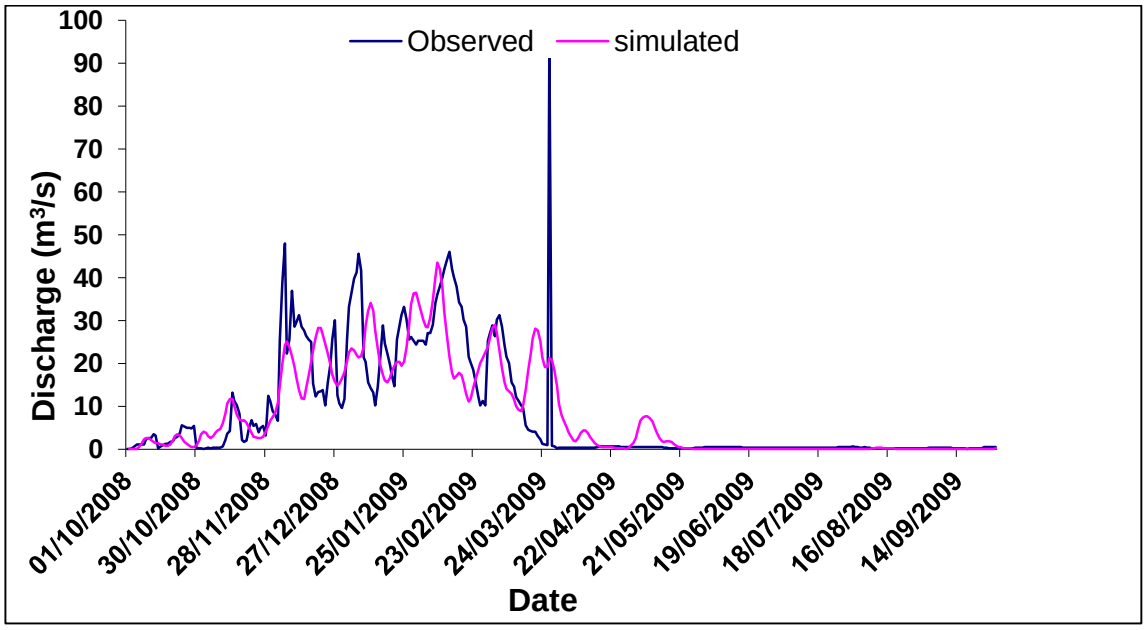

Figure 4-13: Validation Hydrograph for Angwa Catchment

Validation results for Angwa Catchment (Figure 4-13) gave a RBIAS of -0.003 % and a Nash-Sutcliffe coefficient of 0.704 indicating an acceptable model performance. The hydrograph shows a peak flow which the model failed to simulate. The peak could be due to private dams in the upstream catchments whose control is also private. Table 4.7 shows the summary of model efficiencies after validation.

Table 4.7: Summary of the model efficiencies for catchment validations

Catchment (STATION)	NSE	RBIAS (%)	RRMSE (%)
Musengezi (C109)	0.361	0.036	5.249
L. Manyame(Mapomha)	-0.008	0.071	5.249
Angwa (Angwa)	0.704	-0.003	3.936

4.3.2 HEC-RAS flood routing

Based on the hydrographs from the rainfall-runoff model for Lower Manyame, as well as the statistically predicted flows using the Gumbel distribution, steady flow simulations were performed for 2008-2009 hydrological season , return periods of 10, 25, 50 and 100 years. Table 4.8 shows the statistically predicted flows using the Gumbel distribution. The results show that flows increase with the Gumbel y variate as well as with different return period floods. A 100 year return flood gives the highest flows. Flows are higher in the Ambi tributary due to the large micro-catchment area compared to downstream flows contributed by a smaller micro-catchment.

Table 4.8: Gumbel distribution flows

Return period	Probability (%)	Gumbel y variate	Ambi (m^3/s)	Upstream (m^3/s)	Downstream (m^3/s)
10	10	2.25	260.78	233.58	138.71
25	4	3.199	344.59	313.25	187.06
50	2	3.902	406.68	372.26	222.87
100	1	4.6	468.32	430.85	258.43

The following are the model results in the form of profile plots and 3D views. Knowledge of the river stations is essential fin understanding the hydraulic modeling results. The stations

outline the location of each cross section along the modeled reach according to their distance to the downstream outlet.

Figures 4-14, 4-15 and 4-16 are cross sections taken at representative points along the three reaches, that is for the tributary (Ambi), upstream and downstream respectively. The direction of cross sections is towards downstream.

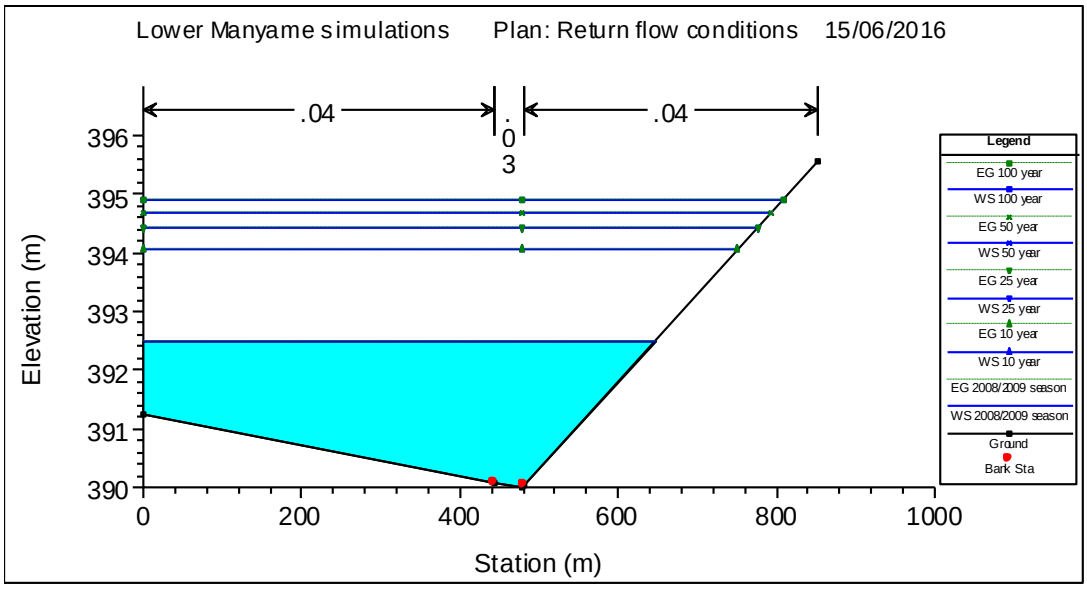

Figure 4-14: Cross section at staion 24863.36 Ambi trbutary

From the cross section (Figure 4-14) on the tributary Ambi, it can be seen that the waterway does not have adequate capacity to transport the peak discharge of the 2008-2009 season of 212 m^3/s even up to 100 year flood in this part of the channel. From calibrations, the channels, upstream, downstream and the tributary can accommodate flows less than 50 m^3/s. In the 2005-2006, 2013-2014 and 2014-2015 recorded flood years, the recorded peak flows exceeded 50 m^3/s. The channels' incapabilities to convey flood flows could be due to accumulation of sediments from upstream as well as sediments from backwaters making them shallow and hence fail to convey flows.

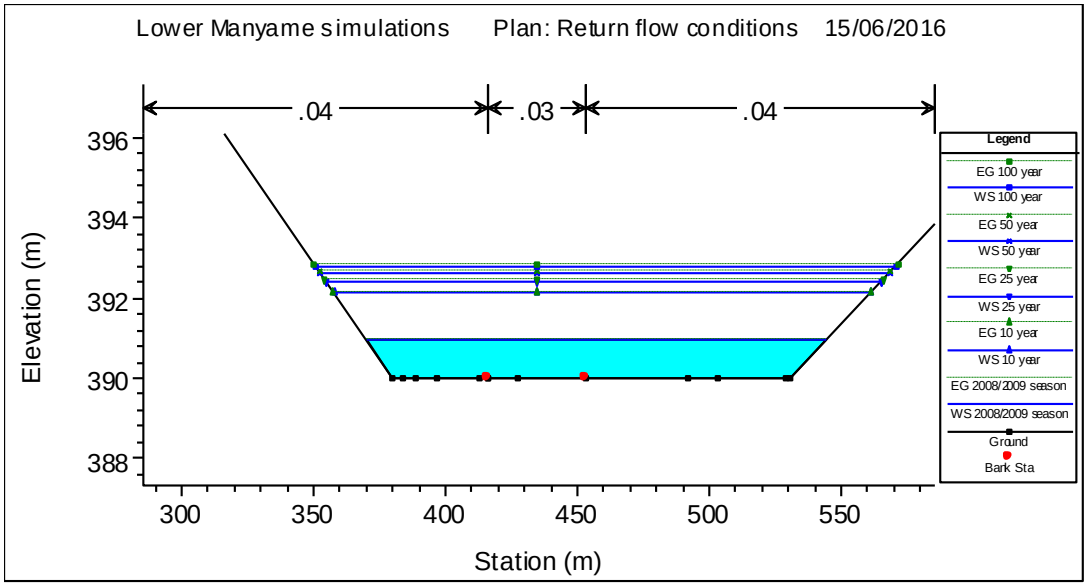

Figure 4-15: Cross section view Upstream of Manyame River

The cross sections for Manyame upstream (Figure 4-15) and Manyame downstream (Figure 4-16) also shows the incapability of the river channel at these sections to convey flood flows hence this helps explain the flood event in 2008 to 2009 season. The fact that the 2008-2009 season flood and the return period floods are higher than the left and right channels for the three reaches indicates that the risk of lateral outflow at these sections is high.

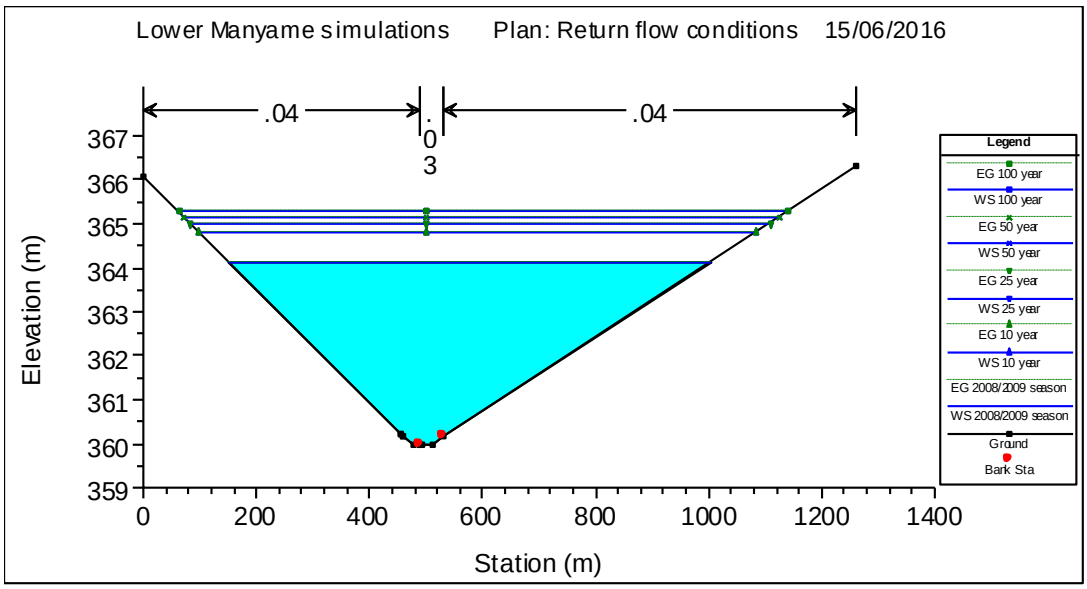

Figure 4-16: Cross section view downstream of Manyame River

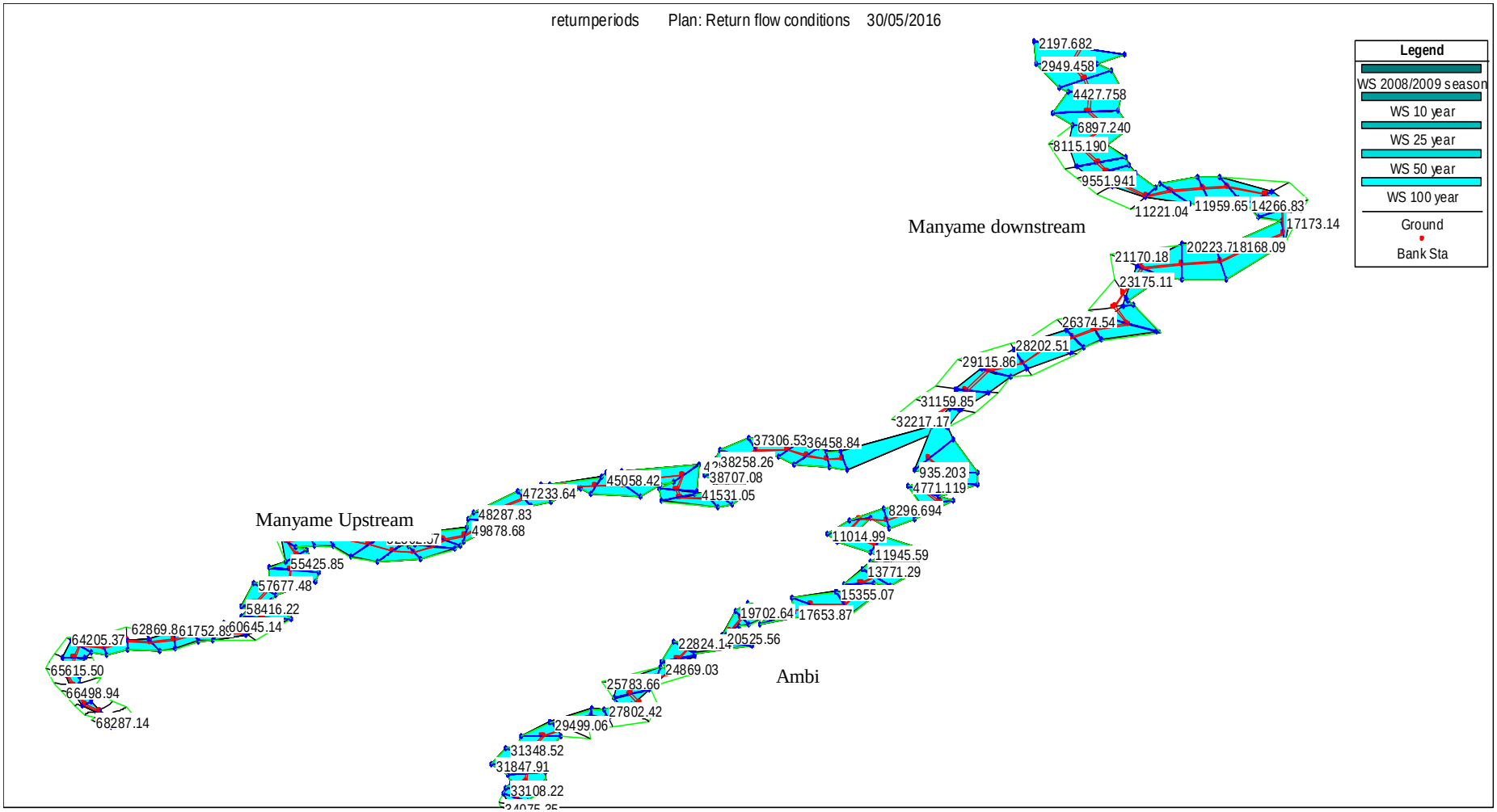

Figure 4-17: x-y-z profile for all reaches

Figure 4-17 shows the 3 D view of the reaches upstream, downstream and the tributary Ambi. Shown are the cross sections and their stations. The 100 year return flood is more significant hence communities need to be prepared for such flows through feasible flood management practises.

Table 4.9: Detailed HEC-RAS output table for 2008-2009 Season RS 28702.51 and RS 25703.67

Element	Left OB	Channel	Right OB	Left OB	Channel	Right OB
Wt. n-Manning.	0.04	0.03	0.04	0.04	0.03	0.04
Reach Len. (m)	637.48	1030.77	1235.56	487.84	847.42	975.54
Flow Area (m^2)	**1409.37**	**125.84**	**136.32**	**187.17**	**143.55**	**1545.44**
Area (m^2)	**1409.37**	**125.84**	**136.32**	**187.17**	**143.55**	**1545.44**
Flow (m^3/s)	26.08	2.7	1.23	1.61	2.9	25.49
Top Width (m)	**534.2**	**58.91**	**152.32**	**168.28**	**55.41**	**522.93**
Average. Velocity. (m/s)	0.02	0.02	0.01	0.01	0.02	0.02
Hydraulic. Depth (m)	2.64	2.14	0.89	1.11	2.59	2.96
Conveyance. (m^3/s)	67270.7	6957	3164.8	5023.1	9025.1	79434.1
Wetted Per. (m)	534.24	58.92	152.33	168.29	55.41	524.24
Cum Volume (1000 m^3)	6150.36	1197.04	9176.76	4741.66	786.92	7033.26
Cum Surface Area (1000 m^2)	10352.8	1249.99	12500.33	9669.53	1124.52	11480.71

Table 4.9 shows details at two stations, RS 28202.51 and RS 25703.67 downstream of Manyame River. To note is the flow area which is the lateral flow from the channel. The stations were chosen as they represent the maximum areas for both the Left overbank (OB) and Right OB. The average flow area is about 1 477 km^2 and average width of 528 m for both overbanks for the 2008-2009 flood event.

Table 4.10: Output table for 100 year return flood RS 2179.682

Element	Left OB	Channel	Right OB
Wt. n-Manning	0.04	0.03	0.04
Flow Area (m^2)	122.75	5.08	114.27
Area (m^2)	122.75	5.08	114.27
Flow (m^3/s)	130.1	7.19	121.12
Top Width (m)	**1052.98**	**43.61**	**980.29**
Avg. Vel. (m/s)	1.06	1.41	1.06
Hydraulic. Depth (m)	0.12	0.12	0.12
Conv. (m^3/s)	732.2	40.4	681.7
Wetted Per. (m)	1053.1	43.61	980.41

The RS 2179.682 (Table 4.10) was chosen as it had the largest flow width for the 100 year return flood on both the left bank and right bank. The average width is about 1000 m from the river channel that was flooded

Figure 4-18 shows the different water surface profiles of the flood inundated areas. It can be noted that in areas with lowest elevation, the area inundated is large thus confirming that elevation can help explain flooding in the district. The 100 year return flood covers the largest area of 59.5 km^2 and at some representative stations the lateral flow covers almost 1 000 m. The computed inundated areas for the return periods are shown in Table 4.11. It is evident that the floodplain inundated areas increase with magnitude of flow confirming the high flood hazard level for settlements and activities near river networks in the district.

Sarhadi et al. (2012) carried out a study in Halilrud basin in Iran, and used HEC-RAS to map flood inundated area for a 1993 flood of magnitude of 3800 m^3/s. The flood was declared a 1000 year return flood. In their study, the area inundated was 73.15 km^2 and a width of 496.6m.

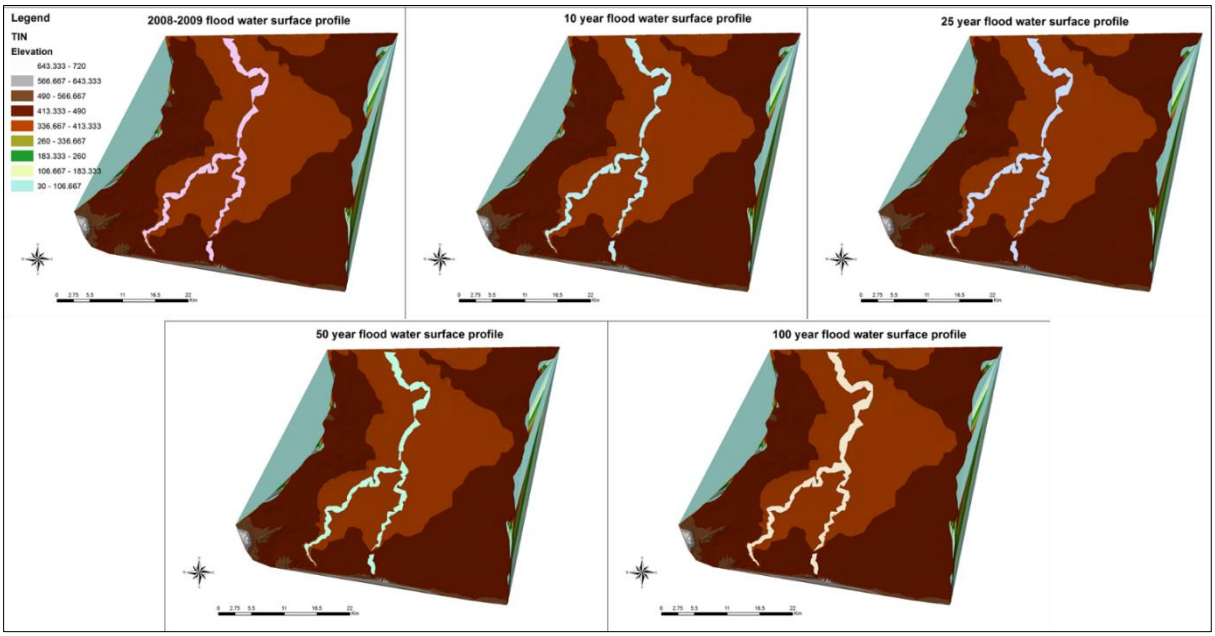

Figure 4-18: Flood water surface profiles for different flood return periods

Table 4.11: Areas inundated

	2008-2009 Season	**10 year flood**	**25 year flood**	**50 year flood**	**100 year flood**
Area (km^2)	56.3	57.93	58.45	58.7	59.1

Validation of HEC-RAS derived flooded areas

Cohen's KAPPA, showed a significant measure of agreement ($p<0.05$) of 0.77 between the 39 ground control points and the inundated areas simulated by the HEC-RAS model. The results show that the model was able to simulate the flood inundated areas well since more than 75 % of the ground control points fall within the HEC-RAS flooded area. However, the model might have performed better if current flow data, for 2014-2015 flood season was compared to the ground control points collected in December 2015.

The flooded areas are in Mushumbi Pools, Chikafa and Hunyani. These results can be used by relevant Mbire authorities in floodplain management as well as communities to better cope with flooding events.

CHAPTER FIVE: CONCLUSIONS AND RECOMMENDATIONS

Conclusions

Based on the findings of this study the following conclusions can be drawn:

1. The Mbire District is prone to repeated floods nearly every season. Using just the years identified by CPU and ZINWA, Remote Sensing was used to calculate inundated areas of different flood events. The results indicated that 16 January 2006 had the greatest inundated area of 1934 km^2 covering the lower part of Ambi tributary, the whole of Upper Manyame River (Dande), Kadzi River and parts of Musengezi River. The second largest area flooded (1 895 km^2) was on 8 January 2015 covering the downstream areas of Ambi tributary, downstream of Manyame River, Mwanzamutanda River as well as part of Kadzi River. It can thus be concluded that remote sensing provides the best potential to analyse the flood extent areas required for operational use in planning flood related emergency responses.

2. Using geostatistical modeling and the inundated areas, areas of different flood hazard zones including flood safe areas in Mbire District were established. The results indicated that distance from dams significantly explained ($p<0.05$) the probability of flooding for 1 day and distance from rivers significantly explained flood probability for 2 days. However TPI, vertical channel height could not significantly explain ($p<0.05$) the probability of flooding for the remotely sensed observed days. The results show that distance from dam and distance from rivers are stable parameters in understanding what may cause flooding in the district.

    a. Therefore it can be deduced that distance from dams as also proved by Phiri (2011) in his study were he concluded that when Cahora Bassa Lake water level exceed 318m they contribute to flooding in this study area from backflows. Distance from the stream networks plays a significant role in explaining flooding as well as landcover and soils.

    b. With the flooded areas established, flood hazard maps were produced to provide crucial information that can minimise the loss of lives, property caused by future floods. This leads to the conclusion that geospatial techniques

and remote sensing provide the best potential to analyse flood extent areas required for prompt and effective decision-making on floods.

3. Based on a five year rainfall-runoff simulation results using HEC-HMS model, it can be deduced that HEC-HMS can be a dependable tool to model river flows. The analysis have also found that HEC-HMS can be used to generate missing data and estimate flood from rainfall data. The peak flows from the modeled years occurred in 2008 – 2009 season. Hence the derived HEC-HMS model can be used as an effective tool to predict flowrates for design purposes.

4. The flood hazard analysis using HEC-RAS confirmed that distance from rivers helps explain flooding in the district. The 2008-2009 flood event covered an average width of 500 m on both banks and the simulated 100 year return flood had an average width of 1000 m from the river channel. This shows that areas of settlements and agricultural fields within a kilometre from the river networks are exposed to a high level of flood related threat. For a flood magnitude exceeding 50 m^3/s, settlements within 200 m will be affected. The artificial channel was found to mark the beginning of the zones with highest hazard. Lateral outflow of flood runoff in the area of Mushumbi, Chikafa and parts of Chidodo is likely as also predicted by the binary logistic model.

Recommendations

In view of these conclusions, the following recommendations are suggested:

1. An analysis of categorised factors to explain flooding in the district
2. Application of the hydraulic model to further calculate inundated areas for the other two catchments in Angwa and Musengezi and validation using probabilistic flood inundation modeling techniques or observed data.
3. Future studies should predict when the next flood event will possibly occur and take into account climate change.
4. Development of a flood protection measure framework showing practical and practical solutions for the protection of the settlements and agricultural fields against 100 year flood.

5. Future studies in the area need to do an extensive soil analysis and track soil composition changes due to flooding depositions
6. If the flood hazard condition is controlled by sufficient drainage infrastructure, a flood emergency management strategy would be implemented for the settlements. The design should contain communication strategies of the flood risk with the communities, a flash flood warning system as well as an emergency evacuation plan. The emergency strategy should clearly show the areas that are to be evacuated when flooding is predicted as well as shelters in the closer area that are not exposed to flood hazard.

6.0 References

(DREF), Disaster Relief Emergency Fund, 2011. Namibia Floods.

(FAO), Food and Agriculture Organization of the United Nations, 2009. HARMONIZED WORLD SOIL DATABASE in: FAO (Ed.), 1.1 ed, ROME, ITALY, AUSTRIA.

(HEC), U. S. Army Corps of Engineers.H.E.C., 2008. HEC-RAS, River Analysis System Hydraulic Reference Manual.

(http://modis.gsfc.nasa.gov/). 2008. MODIS NDVI Datasets.Accessed 10January 2016

Abebe, A.N., Ogden, F.L., Pradhan, N.R., 2010. Sensitivity and uncertainity analysis of the conceptual HBV rainfall-runoff model:Implications for parameter estimation. Journal of Hydrology 389, 301-310.

Adejeji, A.A., Salami, A.W., 2008. Environmental hazard: Flooding and Its Effects on Residential Buildings in Ilorin, Nigeria, Nigeria.

Artur, L., Hilhorst, D., 2014. Floods, resettlement and land access and use in the Lower Zambezi, Mozambique. Land Use Policy 36, 361-368.

Aryal, K.S., Bates, B.C., 2008. Effects of catchment discretization on topographic index distributions. Journal of Hydrology 359, 150-163.

Azagra, E., Olivera, F., 1999. Introduction to AVRas. Center for Research in Water Resources.

Bates, P.D., Wilson, M.D., Horritt, M.S., Mason, D.C., Holden, N., Currie, A., 2006. Reach scale floodplain inundation dynamics observed using airborne synthetic aperture radar imagery: Data analysis and modelling. Journal of Hydrology 328, 306-318.

Beck, L., Bernauer, T., 2010. Water Scenarios for the Zambezi River Basin, 2000 - 2050.

Beilfuss, R., 2001. Patterns of Hydrological Change in the Zambezi Delta, Mozambique. Program for the Sustainable Management of Cahora Bassa Dam and the Lower Zambezi Valley.

Bengtson, M.L., Padmanabhan, G., 2000. A Review of Models for Investigating the Influence of Wetlands on Flooding. International Joint Commission Red River Task Force.

Bola, G., Mabiza, C., Goldin, J., Kujinga, K., Nhapi, I., Makurira, H., Mashauri, D., 2014. Coping with droughts and floods: A Case study of Kanyemba, Mbire District, Zimbabwe. Physics and Chemistry of the Earth, Parts A/B/C 67–69, 180-186.

Brunner, G.W., 2008. HEC-RAS, River Analysis System Hydraulic Reference Manual. US ARMY CORPS OF ENGINEERS HYDROLOGIC ENGINEERING CENTER (HEC).

Brunner, G.W., 2010. HEC-RAS, River Analysis System Hydraulic Reference Manual. US ARMY CORPS OF ENGINEERS HYDROLOGIC ENGINEERING CENTER (HEC).

Cameron, T., Ackerman, P.E., 2009. HEC-GeoRAS GIS Tools for Support of HEC-RAS using ArcGIS User's Manual. US Army Corps of Engineers Institute for Water Resources Hydrologic Engineering Center (HEC).

Chen, X., Xu, Y., Yin, Y., 2009. Impacts of land use change scenarios on storm-runoff generation in Xitiaoxi basin, China. Quaternary International 208, 121-128.

Costabile, P., Macchione, F., 2015. Enhancing river model set-up for 2-D dynamic flood modelling. Environmental Modelling & Software 67, 89-107.

Cupal, M., Deev, O., Linnertova, D., 2015. The Poisson Regression Analysis for Occurence of Floods. Procedia Economics and Finance.

Czigany, S., Pirkhoffer, E., Geresdi, I., 2010. Impact of extreme rainfall and soil moisture on flash flod generation. Journal of the Hungarian Meteorological Services 114, 79-100.

Daniel, T.C., Vining, J., 1983. Methodological Issues in the Assessment of Landscape Quality. . Plenum Press.
Dottori, F., Salamon, P., Bianchi, A., Alfieri, L., Hirpa, F.A., Feyen, L., 2016. Development and evaluation of a framework for global flood hazard mapping. Advances in Water Resources 94, 87-102.
Dube, F., Nhapi, I., Murwira, A., Gumindoga, W., Goldin, J., Mashauri, D.A., 2014. Potential of weight of evidence modelling for gully erosion hazard assessment in Mbire District – Zimbabwe. Physics and Chemistry of the Earth, Parts A/B/C 67–69, 145-152.
Elkhrachy, I., 2015. Flash Flood Hazard Mapping Using Satellite Images and GIS Tools: A case study of Najran City, Kingdom of Saudi Arabia (KSA). The Egyptian journal of Remote Sensing and Space Sciences 18, 267-278.
Emerton, L., 2003. Barotse Floodplain, Zmbia: local economic dependence on wetland resources.
Evans, S.Y., Gunn, N., Williams, D., 2007. Use of GIS in Flood Risk Mapping.
Ganova, L., 2003. Floods - their definition, causes, consequences and state of the art. LLP IP Erasmus, 1-26.
Garcia, M.L., Basile, P.A., Riccardi, G.A., Rodriguez, J.F., 2015. Modelling extraordinary floods and sedimentological processes in a large channel-floodplain system of the Lower Paraná River (Argentina). International Journal of Sediment Research 30, 150-159.
Guan, M., Carrivick, J.L., Wright, N.G., Sleigh, P.A., Staines, K.E., 2016. Quantifying the combined effects of multiple extreme floods on river channel geometry and on flood hazards. Journal of Hydrology 538, 256-268.
Gumindoga, W., 2008. THE SPATIAL VARIATION OF FLOOD HAZARD IN THE CHOBE-CAPRIVI WETLAND SYSTEM OF THE UPPER ZAMBEZI BASIN, Geography and Environmental Science. University of Zimbabwe, p. 58.
Gumindoga, W., 2012. Runoff Simulation For The Upper Manyame Catchment Using The HEC-HMS, Harare.
Gumindoga, W., Chikodzi, D., Rwasoka, D.T., Mutowo, G., Togarepi, S., Dube, T., 2014a. The Spatio-Temporal Variation of the 2014 Tokwe-Mukosi Floods: A GIS and Remote Sensing Based Approach. Journal of Science, Engineering & Technology 2, 1-10.
Gumindoga, W., Rientjes, T.H.M., Haile, A.T., Dube, T., 2014b. Predicting streamflow for land cover changes in the Upper Giilgel Abay River Basin, Ethiopia: A TOPMODEL based approach. Physics and Chemistry of the Earth 76-78, 3-15.
Halwatura, D., Najim, M.M.M., 2013. Application of the HEC-HMS model for runoff simulation in a tropical catchment. Environmental Modelling & Software 46, 155-162.
HEC, H.E.C., 2000. Hydrologic Modeling System HEC-HMS Technical Reference Manual. U.S. Army Corps of Engineers, U.S.A.
HEC, H.E.C., 2009. Hydraulic Reference Manual. U.S ARMY CORPS OF ENGINEERS HYDROLOGIC ENGINEERING CENTER (CA).
HEC, H.E.C., 2010b. HEC-RAS Hydraulic Reference Manual,. U. S. Army Corps of Engineers Hydrologic Engineering Center.
Heimhuber, V., 2013. GIS Based Flood Modeling as Part of an Integrated Development Strategy for Informal Settlements: A Case study in Applying GIS(ArcMap) in Combination with Hydrologic (HEC-HMS) and Hydraulic (HEC-RAS) Modeling to Estimate teh Flood Hazard of Onaville - Canaan- Haiti, Urban Water Systems Engineering. Technische Universitat Munchen, Munich.

Islam, M., Sado, K., 2000. Satellite Remote Sensing Data Analysis for Flood Damaged Zoning with GIS for Flood Management. Hydraulic Engineering 44, 1-6.
Jensen, J.R., Lulla, K., 1987. Introductory digital image processing: a remote sensing perspective.
Jonkman, S.N., 2005. Global Perspectives on Loss of Human Life Caused by Floods. 151–175.
Jovel, R., Muraya, F., Wielinga, D.G., Lemoine, G., Gerhardinger, A., Andriamihaja, A., 2009. Post-Disaster Needs Assessment Namibia. Government of the Republic of Namibia, Namibia.
Kampata, J.M., Parida, B.P., Moalafhi, D.B., 2008. Trend analysis of rainfall in the headstreams of the Zambezi River Basin in Zambia. Physics and Chemistry of the Earth 33, 621-625.
Karmakar, S., 2010. Hydrologic Simulation Models.
Khanna, R.K., Agrawal, C.K., Kumar, P., 2005. Remote Sensing and Gis Applications in Flood Management. 1 - 11.
Kindon, S., Pain, R., Kesby, M., 2010. Participatory Action Research Approaches and Methods: Connecting People, Participation and Place. Participatory Learning and Action on participatory mapping and GIS.
Knebl, M.R., Yang, Z.L., Hutchison, K., Maidment, D.R., 2005. Regional scale flood modeling using NEXRAD rainfall, GIS, and HEC-HMS/RAS: a case study for the San Antonio River Basin Summer 2002 storm event. Journal of Environmental Management 75, 325-336.
Kundzewicz, Z.W., Kanae, S., Seneviratne, S.I., Handmer, J., Nicholls, N., Peduzzi, P., Maechler, R., Bouwer, L.M., Arnell, N., Mach, K., Muir-Wood, R., Brakenridge, R., Kron, W., Benito, G., Honda, Y., Takahashi, K., Sherstyukov, B., 2014. Flood Risk and climate Change:Global and Regional Perspectives. Hydrological Sciences 59, 1-28.
Lawal, D.U., Matori, A., Hashim, A., Chandio, I.A., 2011. Geographic Information System and Remote Sensing Applications in Flood Hazards Management: A Review. Research Journal of Applied Sciences, Engineering and Technology 3, 933-947.
Leonard, B., 2009. Floods:The Awesome Power. NOAA.
Lydersen, S., 2014. Measuring agreement between raters. Regional Centre for Child and Youth Mental Health and Child Welfare.
Maathuis, B.H.P., 2006. Digital Elevation Model Based Hydro-processing. Geocarto International 21, 21-26.
Madamombe, E., 2004. The Associated Programme on Flood Management Integrated Flood Management
Madamombe, E., 2006. Zimbabwe: flood Management Practices-Selected Flood Prone Areas Zambezi Basin. Water Resources.
Mavhura, E., Manyena, S.B., Collins, A.E., Manatsa, D., 2013. Indigenous knowlegde, coping startegies and resilience to floods in Muzarabani, Zimbabwe. International Journal of Disaster Risk Reduction 5, 38-48.
Merkuryeva, G., Merkuryev, Y., Sokolov, B.V., Potryasaev, S., Zelentsov, V.A., Lektauers, A., 2015. Advanced river flood monitoring, modelling and forecasting. Journal of Computational Science 10, 77-85.
Miller, J.F., Frink, D.L., 1984. Changes in Flood Response of the Red River of the North Basin, North dakota-Minnesota, Geological Survey water-supply paper: 2243. Upper Mississippi River Basin Commission.

Moriasi, D.N., Arnold, J.G., Van Liew, M.W., Bingner, L.R., Harmel, D.R., Veith, T.L., 2007. Model Evaluation Guidelines for Systematic Quantification of Accuracy in Watershed Simulations, in: USDA-ARS (Ed.), Soil and Water Division.

Muhonda, P., Mabiza, C., Makurira, H., Kujinga, K., Nhapi, I., Goldin, J., Mashauri, D.A., 2014. Analysis of institutional mechanisms that support community response to impacts of floods in the middle-zambezi river basin, Zimbabwe. Physics and Chemistry of the Earth, Parts A/B/C 76–78, 64-71.

Mujere, N., 2011a. Flood Frequency Analysis using the Gumbel Distribution. International Journal on Computer Science and Engineering (IJCSE) 3, 2774-2778.

Mujere, N., 2011b. Flood Frequency Analysis Using the Gumbel Distribution. International Journal on Computer Science and Engineering (IJCSE) 3, 1-5.

Mulugeta, G., Ayonghe, S., Dube, O.P., Gudyanga, F., Lucio, F., Durrheim, R., 2007. Natural and Human-induced Hazards and Disasters in sub-Saharan Africa. ICSU ROA Science Plan.

Murwira, A., Schmidt-Murwira, K.S., 2005. A GIS and Remote Sensing based Flood Warning System for Muzarabani: Zambezi Catchment, Harare.

Mwale, F.D., Adeloye, A.J., Beevers, L., 2015. Quantifying vulnerability of rural communities to flooding in SSA: A contemporary disaster management perspective applied to Lower Shire Valley, Malawi. Journal of Disaster Risk Reduction 12, 172-187.

NASA.GOV, 2010. MODIS Rapid Response System.

Nash, J.E., Sutcliffe, J.V., 1970. River flow forecasting through conceptual models part 1 - A discussiion of principles. Journal of Hydrology 10, 282-290.

Nath, B., Lillicrap, A.M., Ellis, L.C., Boland, D.D., Oldham, C.E., 2013. Hydrological and chemical connectivity dynamics in a groundwater-dependent ecosystem impacted by acid sulfate soils,. Water Resources Research 49, 441-457.

Nations, F.a.A.O.o.t.U., 2015. World reference base for soil resources 2014. Food and Agriculture Organization of the United Nations, Italy, Rome.

Neal, J.C., Odoni, N.A., Trigg, M.A., Freer, J.E., Garcia-Pintado, J., Mason, D.C., Wood, M., Bates, P.D., 2015. Efficient incorporation of channel cross-section geometry uncertainty into regional and global scale flood inundation models. Journal of Hydrology 529, Part 1, 169-183.

Nelson, S.A., 2001. Streams and Drainage Systems. Channels, 1 - 10.

Nelson, S.A., 2012. River Systems & Causes of Flooding. Natural Disasters, 1-13.

Nilsson, C., Berggren, K., 2000. Alterations of Riparian Ecosystems Caused by River Regulation. BioScience 50, 783-793.

NRCS, N.R.C.S., 1986. Urban Hydrology for small watersheds.

Ogawa, H., Male, J.W., 1986. Simulating the Flood Mitigation Role of Wetlands. Journal of water Resources Planning and Management 112, 114-118.

Osti, R., Tanaka, S., Tokioka, T., 2008. Flood hazard mapping in developing countries: problems and prospects", . Disaster Prevention and Management 17pp. , 104 - 113.

Papathanasiou, C., Makropoulos, C., Mimikou, M., 2015. Hydrological modelling for flood forecasting: Calibrating the post-fire initial conditions. Journal of Hydrology.

Pappenberger, F., Beven, K., Horritt, M., Blazkova, S., 2005. Uncertainty in the calibration of effective roughness parameters in HEC-RAS using inundation and downstream level observations. Journal of Hydrology 302, 46-69.

Phiri, M., 2011. Analysis of the Cahora Bassa Dam Water Balance and Impact of Reservoir Operations on Upstream Settlements.

Reed, B., Budde, M., Spencer, P., Miller, E.A., 2009. Integration of MODIS-derivedmetrics to assess interannual variability in snowpack, lake ice, and NDVI in Southwest Alaska. Remote Sensing of Environment, 2-3.
Rodriguez, J., below, R., Guha-Sapir, D., 2009. Annual Disaster Statistical Review.
Sanyal, J., Lu, X.X., 2004. Application of Remote Sensing in Flood Management with Special Reference to Monsoon Asia. Natural Hazards 33, 283-301.
Sarhadi, A., Soltani, S., Modarres, R., 2012. Probabilistic flood inudation mapping of ungauged rivers: Linking GIS techniques and frequency analysis. Journal of Hydrology 458-459, 68-86.
Shela, N.O., 2012. A proposal to improve The Flood Forecasting and Early Warning System (Limpopo River Basin). World Meteorological Organisation.
Shumba, S., Makurira, H., Nhapi, I., Gumindoga, W., 2014. Environmental Impacts of Natural and Man-Made Hydraulic Structures- Case Study Middle Zambezi Valley, Zimbabwe. International Journal of Application or Innovation in Engineering & Management 3, 1 - 16.
Simpson, J.J., Stitt, J.R., Sienko, M., 2008. Improved estimates of the areal extent of snow cover from AVHRR data. Journal of Hydrology 204, 1-23.
Sitoe, S.R., Risberg, J., Norstrom, E., Snowball, I., Holmgre, K., Achimo, M., Mugabe, J., 2015. Paleo-environment and flooding of the Limpopo River-plain, Mozambique, between c. AD 1200-2000. CATENA 126, 105-116.
Smith, C.L., 1997. Satellite Remote Sensing of River Inundation Area, Stage and Disharge: A Review. Hydrological Processes 11, 1427-1439.
Thoms, M.C., Southwell, M., McGinness, H.M., 2005. Floodplain–river ecosystems: Fragmentation and water resources development. Geomorphology 71, 126-138.
United Nations., 2009. Water in a Changing World, The Unied Nations World Water Development UNESCO, Paris, London.
Vilches, P.J., 2013. Detection of Areas Affected by Flood River using SAR images.
Wang, Y., Colby, J.D., Mulcahy, K.A., 2002. An efficient method for mapping flood extent in a coastal floodplain using Landsat TM and DEM data. International Journal of Remote Sensing 23, 3681-3696.
Warner, J.C., Brunner, G.W., Wolfe, B.C., Piper, S.S., 2010. HEC-RAS, River Analysis System Applications Guide. US ARMY CORPS OF ENGINEERS HYDROLOGIC ENGINEERING CENTER (HEC).
William, A., Scharffenberg, Fleming, M.J., 2008. Hydrologic Modeling System HEC-HMS User's Manual. U.S.Army Corps of Engineers Hydrologic Engineering Center, HEC.
World Bank., 2006. Hazards of Nature,Risks to Development An IEG Evaluation of World Bank Assistance for Natural Distasters.
World Bank., 2010. The Zambezi River Basin A Multi-Sector Investment Opportunities Analysis. The World Bank, USAXu, C., 2002. Hydrologic Models. Uppsala University, Department of Earth Sciences Hydrology, Sweden.
World Meteorological Organization., 2013. Flood Mapping. Integrated Flood Management Tools Series. 88.
Zazo, S., Molina, J.-L., Rodríguez-Gonzálvez, P., 2015. Analysis of flood modeling through innovative geomatic methods. Journal of Hydrology 524, 522-537.
Zhang, Q., Gu, X., Singh, P.V., Chen, X., Xiao, M., 2015. Evaluation of flood frequency under non-stationary resulting from climate indices and reservoir indices in the East River Basin, China. Journal of Hydrology 527, 565-575.
Zhang, Y., Zhang, H., Lin, H., 2014. Improving the impervious surface estimation with combined use of optical and SAR remote sensing images. Remote Sensing of Environment 141, 155-167.

ZimStat, 2012. Zimbabwe Population Statistics.

7.0 Appendices

Appendix A: MODIS DERIVED FLOODS

APPENDIX A 1: MODIS LOOK UP TABLE

Colour			NDVI
R	G	B	
153	204	255	<=0.0
225	175	100	0.0-0.1
255	225	150	0.1-0.2
225	255	175	0.2-0.3
152	255	152	0.3-0.4
102	255	102	0.4-0.5
51	204	51	0.5-0.6
0	153	0	0.6-0.7
0	102	0	>0.7
255	255	255	no data

APPENDIX A 2: MODIS FLOOD ARE DERIVATION SCRIPT

Water_red_222:=iff(red_222=154,1,0)

Water_green_222:=iff(green_222>210,0,iff(green_222<180,0,1))

Water_blue_222:=iff(blue_222<200,0,1)

Water_222:=water_red_222+water_green_222+water_blue_222

Flood_222:=iff(water_222>1,1,0)

Appendix B: FACTORS AFFECTING FLOODS

APPENDIX B 1: ALGORITHMS AND PROBABILITY MAPS EXPLAINING FLOODING AND TPI

Date	Variables	B	Sig.	Equation
02/01/14	TPI	0.279	0.047	P=exp(-0.407+0.279*tpi)/(1+exp(-0.407+0.279*tpi))
	Constant	-0.407	0.884	
12/03/14	TPI	0.250	0.038	P=exp(-4.307+0.250*tpi)/(1+exp(-4.307+0.250*tpi))
	Constant	-4.307	0.088	

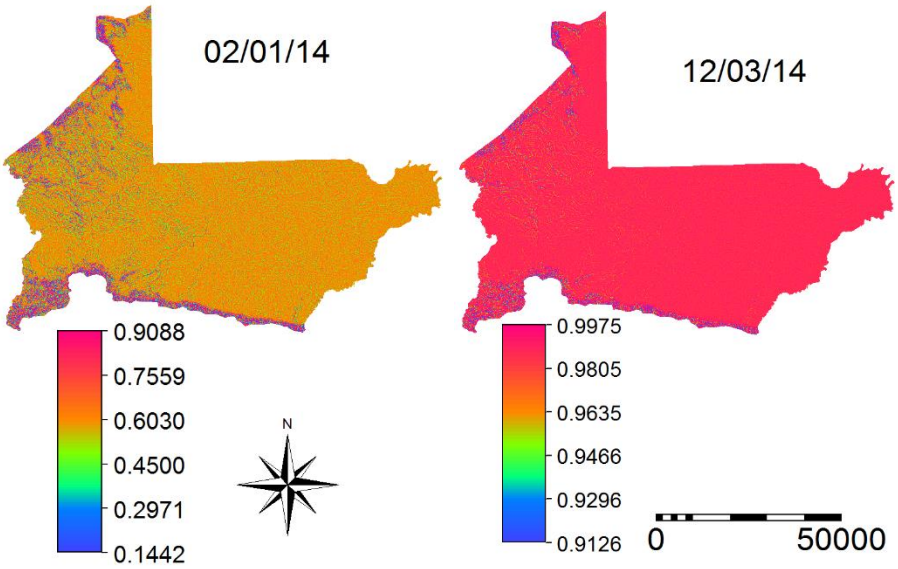

Flood hazard for Mbire District explained by TPI

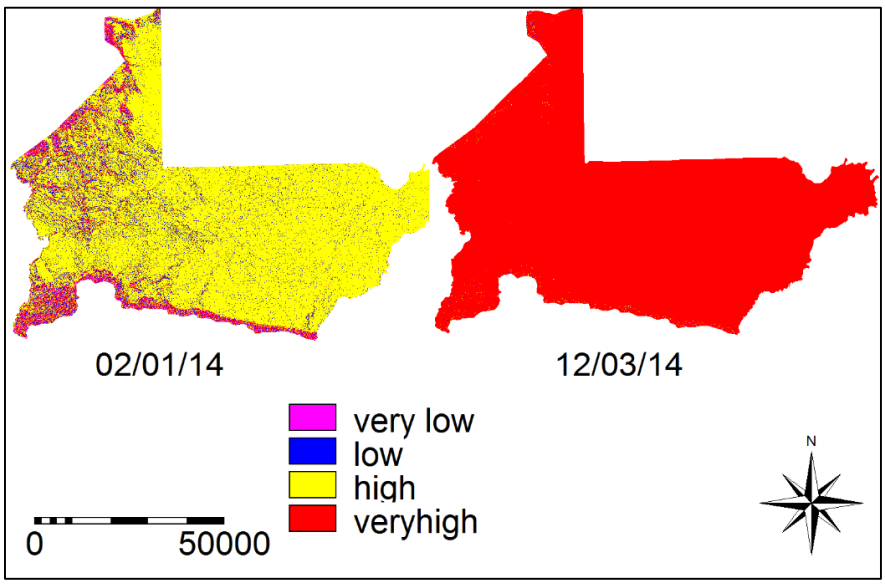

APPENDIX B 2: ALGORITHMS EXPLAINING FLOODING AND ELEVATION

Date	Variables	B	Sig.	Equation
17/01/06	Elevation	0.099	0.002	P=exp(-113.574+0.099*elev)/(1+exp(-
	Constant	-113.574	0.989	113.574+0.099*elev))
2005-06	Elevation	0.006	0.017	P=exp(-1.345+0.006*elev)/(1+exp(-1.345+0.006*elev))
Season	Constant	-1.345	0.368	
17/12/08	Elevation	0.019	0.029	P=exp(-26.392+0.019*elev)/(1+exp(-26.392+0.019*elev))
	Constant	-26.392	0.999	
22/12/08	Elevation	0.024	0.002	P=exp(-5.862+0.024*elev)/(1+exp(-5.862+0.024*elev))
	Constant	-5.862	0.095	
12/03/14	Elevation	0.009	0.028	P=exp(-4.307+0.009*elev)/(1+exp(-4.307+0.009*elev))
	Constant	-4.307	0.088	
09/01/15	Elevation	0.015	0.029	P=exp(-14.256+0.015*elev)/(1+exp(-14.256+0.015*elev))
	Constant	-14.256	0.999	

APPENDIX B 3: ALGORITHMS EXPLAINING FLOODING AND DISTANCE FROM DAMS

Date	Variables	B	Sig.	Equation
17/01/06	Distance_dams	0.0001	0.001	P=exp(-17.781+0.0001* DD)/(1+exp(-17.781+0.0001* DD))
	Constant	-17.781	0.999	
22/12/08	Distance_dams	0.000076	0.010	P=exp(-5.862+0.000076* DD)/(1+exp(-5.862+0.000076*
	Constant	-5.862	0.095	DD))
19/01/09	Distance_dams	0.00063	0.003	P=exp(-21.984+0.00063* DD)/(1+exp(-21.984+0.00063*
	Constant	-21.984	1.000	DD))
13/12/13	Distance_dams	0.000165	0.000	P=exp(-9.817+0.000165* DD)/(1+exp(-9.817+0.000165*
	Constant	-9.817	0.211	DD))
12/03/14	Distance_dams	0.000079	0.008	P=exp(-4.307+0.000079* DD)/(1+exp(-4.307+0.000079*
	Constant	-4.307	0.088	DD))
2013-14	Distance_dams	0.000019	0.002	P=exp(-20.037+0.000019* DD)/(1+exp(-20.037+0.000019*
Season	Constant	-20.037	1.000	DD))
07/01/15	Distance_dams	0.000292	0.001	P=exp(-19.72+0.000292* DD)/(1+exp(-19.723+0.000292*
	Constant	-19.723	0.999	DD))
09/01/15	Distance_dams	0.000043	0.046	P=exp(-14.3+0.000043* DD)/(1+exp(-14.3+0.000043* DD))
	Constant	-14.256	0.999	

APPENDIX B 4: ALGORITHMS OF FLOODING AND DISTANCE FROM RIVERS

Date	Variables	B	Sig.	Equation
2005-06	Distance_rivers	0.000212	0.017	P=exp(-0.911+0.000212* DR)/(1+exp(-0.911+0.000212*
Season	Constant	-0.911	0.416	DR))
22/12/08	Distance_rivers	0.001	0.009	P=exp(-5.862+0.001* DR)/(1+exp(-5.862+0.001* DR))
	Constant	-5.862	0.095	
2008-09	Distance_rivers	0.00035	0.000	P=exp(-17.719+0.00035* DR)/(1+exp(-17.719+0.00035*
Season	Constant	-17.719	1.000	DR))
12/03/14	Distance_rivers	0.001	0.010	P=exp(-4.307+0.001* DR)/(1+exp(-4.307+0.001* DR))
	Constant	-4.307	0.088	
2013-14	Distance_rivers	0.000149	0.032	P=exp(-20.037+0.000149* DR)/(1+exp(-20.037+0.000149*
Season	Constant	-20.037	1.000	DR))
09/01/15	Distance_rivers	0.001	0.027	P=exp(-14.256+0.001* DR)/(1+exp(-14.256+0.001* DR))
	Constant	-14.256	0.999	

APPENDIX B 5: ALGORITHMS OF FLOODING AND ELEVATION

Date	Variables	B	Sig.	Equation
22/12/05	Elevation	0.043	**0.006**	P=exp(-17.158+0.043*elev)/(1+exp(-17.158+0.043*elev))
	Constant	-17.158	**0.011**	
02/01/09	Elevation	0.019	**0.002**	P=exp(-12.748+0.019*elev)/(1+exp(-12.748+0.019*elev))
	Constant	-12.748	**0.001**	
07/01/09	Elevation	0.022	**0.011**	P=exp(-12.745+0.022*elev)/(1+exp(-12.745+0.022*elev))
	Constant	-12.745	**0.003**	
03/01/14	Elevation	0.038	**0.007**	P=exp(-27.456+0.038*elev)/(1+exp(-27.456+0.038*elev))
	Constant	-27.456	**0.003**	
21/12/14	Elevation	0.065	**0.005**	P=exp(-41.739+0.065*elev)/(1+exp(-41.739+0.065*elev))
	Constant	-41.739	**0.003**	

APPENDIX B 6: ALGORITHMS OF FLOODING AND VERTICAL CHANNEL HEIGHT (VCH)

Date	Variables	B	Sig.	Equation
17/12/08	VCH	-0.033	**0.05**	P=exp(-30.292+0.05*elev)/(1+exp(-30.292+0.05*elev))
	Constant	-30.292	**0.999**	
19/01/09	VCH	-0.04	**0.002**	P=exp(-28.169+0.02*elev)/(1+exp(-28.169+0.02*elev))
	Constant	-28.169	**0.999**	
16/03/09	VCH	0.342	**0.003**	P=exp(-12.745+0.003*elev)/(1+exp(-12.745+0.003*elev))
	Constant	-12.745	**0.999**	
12/01/14	VCH	-0.038	**0.049**	P=exp(-18.974+0.049*elev)/(1+exp(-18.974+0.049*elev))
	Constant	-18.974	**0.085**	

16/01/15	VCH	-0.027	**0.04**	P=exp(-31.475+0.04*elev)/(1+exp(-31.475+0.04*elev))
	Constant	-31.475	**0.999**	

Appendix C: HEC-HMS SIMULATIONS

APPENDIX C 1: NRCS, MANNING VALUES

Surface description	n [1/]
Smooth surfaces (concrete, asphalt, gravel, or bare soil)	0.011
Fallow (no residue)	0.05
Cultivated soils:	
Residue cover ≤20%	0.06
Residue cover >20%	0.17
Grass:	
Short grass prairie	0.15
Dense grasses [2/]	0.24
Bermudagrass .	0.41
Range (natural)	0.13
Woods:[3/]	
Light underbrush	0.40
Dense underbrush	0.80

[1] The n values are a composite of information compiled by Engman (1986).
[2] Includes species such as weeping lovegrass, bluegrass, buffalo grass, blue grama grass, and native grass mixtures.
[3] When selecting n , consider cover to a height of about 0.1 ft. This is the only part of the plant cover that will obstruct sheet flow.

APPENDIX C 2: GUMBEL DISTRIBUTION TABLE

TABLE A-8 MEAN $\bar{y}_n$ AND STANDARD DEVIATION σ_n OF GUMBEL VARIATE *(y)* VERSUS RECORD LENGTH *(n)*

n	$\bar{y}_n$	σ_n	n	$\bar{y}_n$	σ_n	n	$\bar{y}_n$	σ_n
8	0.4843	0.9043	35	0.5403	1.1285	64	0.5533	1.1793
9	0.4902	0.9288	36	0.5410	1.1313	66	0.5538	1.1814
10	0.4952	0.9497	37	0.5418	1.1339	68	0.5543	1.1834
11	0.4996	0.9676	38	0.5424	1.1363	70	0.5548	1.1854
12	0.5035	0.9833	39	0.5430	1.1388	72	0.5552	1.1873
13	0.5070	0.9972	40	0.5436	1.1413	74	0.5557	1.1890
14	0.5100	1.0095	41	0.5442	1.1436	76	0.5561	1.1906
15	0.5128	1.0206	42	0.5448	1.1458	78	0.5565	1.1923
16	0.5157	1.0316	43	0.5453	1.1480	80	0.5569	1.1938
17	0.5181	1.0411	44	0.5458	1.1499	82	0.5572	1.1953
18	0.5202	1.0493	45	0.5463	1.1519	84	0.5576	1.1967
19	0.5220	1.0566	46	0.5468	1.1538	86	0.5580	1.1980
20	0.5236	1.0628	47	0.5473	1.1557	88	0.5583	1.1994
21	0.5252	1.0696	48	0.5477	1.1574	90	0.5586	1.2007
22	0.5268	1.0754	49	0.5481	1.1590	92	0.5589	1.2020
23	0.5283	1.0811	50	0.5485	1.1607	94	0.5592	1.2032
24	0.5296	1.0864	51	0.5489	1.1623	96	0.5595	1.2044
25	0.5309	1.0915	52	0.5493	1.1638	98	0.5598	1.2055
26	0.5320	1.0961	53	0.5497	1.1653	100	0.5600	1.2065
27	0.5332	1.1004	54	0.5501	1.1667	150	0.5646	1.2253
28	0.5343	1.1047	55	0.5504	1.1681	200	0.5672	1.2360
29	0.5353	1.1086	56	0.5508	1.1696	250	0.5688	1.2429
30	0.5362	1.1124	57	0.5511	1.1708	300	0.5699	1.2479
31	0.5371	1.1159	58	0.5515	1.1721	400	0.5714	1.2545
32	0.5380	1.1193	59	0.5518	1.1734	500	0.5724	1.2588
33	0.5388	1.1226	60	0.5521	1.1747	750	0.5738	1.2651
34	0.5396	1.1255	62	0.5527	1.1770	1000	0.5745	1.2685

Source: Gumbel, E. J. (1958). *Statistics of Extremes.* Irvington, New York: Columbia University Press.